https://doi.org/10.5194/wes-2026-37
Preprint. Discussion started: 17 February 2026
© Author(s) 2026. CC BY 4.0 License.

eawe european academy of wind energy
Open Access WIND ENERGY SCIENCE DISCUSSIONS

Yaw-based wake steering control under field uncertainties: a line of 4 industrial wind turbines investigated with LES and engineering wake models

Etienne Muller[1], Simone Gremmo[2,1], Félix Houtin-Mongrolle[3,4,1], Laurent Beaudet[3], Juliette Coussy[3], Luis A. Martínez-Tossas[5,3], and Pierre Bénard[1]

[1]INSA Rouen Normandie, Univ Rouen Normandie, CNRS, Normandie Univ, CORIA UMR 6614, F-76000 Rouen, France
[2]Von Karman Institute for Fluid Dynamics, Waterloosesteenweg 72 B-1640 Sint-Genesius-Rode, Belgium
[3]Siemens Gamesa Renewable Energy, 685 Avenue de l'Université, 76801 Saint-Etienne-du-Rouvray , France
[4]OWC, 11 rue Arthur III, 44000 Nantes, France
[5]National Laboratory of the Rockies, Golden, Colorado, USA

Correspondence: Etienne Muller (etienne.muller@coria.fr)

Abstract. To enhance the performance of wind farms, the yaw-based wake steering control strategy has emerged as a promising approach and gained increasing attention in the last decade. This study focuses on the classical open-loop implementation of this strategy, which is typically built upon wake models for affordability. The practical robustness of the strategy, with respect to either a static error in the measured absolute wind direction, or a nacelle positioning uncertainty, is assessed. In particular, and while mentioned to be critical in several prior works, the static error in the wind direction is often overlooked. In this work, a real four-turbine offshore layout was simulated under a truly neutral atmospheric boundary layer with the Large Eddy Simulation (LES) coupled code YALES2-BHawC. For the supplementary purposes of comparison and validation, engineering wake models from the FLORIS library were also used to predict the power production, and SCADA data were considered in the baseline case. It was observed that a few-degree static error in the absolute wind direction, which would typically emerge from a calibration bias, is enough in some circumstances to turn a significant expected power benefit into slight losses. Relatively, a typical nacelle position uncertainty only has a marginal impact on the power benefit. When existing, the total power benefit showed to be mainly achieved on the most downstream turbines. Furthermore, despite an overall agreement between the wake models and LES in predicting total power trends, detailed comparisons revealed noteworthy discrepancies related to wake combinations and wake-added turbulence. In particular, it was observed that strong wake overlap conditions result in a significant increase of the meandering amplitude, making it more challenging to get a reliable assessment of the total power benefit on a reasonably short period of time. To ultimately secure a significant power gain, these findings suggest that new efforts remain desirable on the modeling, implementation, and validation sides of open-loop wake steering control.

1 Introduction

Over the past decade, the global installed capacity of wind energy has grown at an average annual rate of 13% (Energy Institute, 2024). To sustain this expansion while further reducing the Levelized Cost of Energy (LCOE), modern wind turbines are

https://doi.org/10.5194/wes-2026-37
Preprint. Discussion started: 17 February 2026
© Author(s) 2026. CC BY 4.0 License.

eawe european academy of wind energy
Open Access WIND ENERGY SCIENCE DISCUSSIONS

increasingly deployed in large-scale wind farms. Originally developed onshore, such farms are now common in the offshore domain as well, which benefits from higher capacity factors (International Energy Agency, 2024). They typically comprise tens to hundreds of turbines operating in close proximity, where the wake of an upstream turbine is likely to impinge on those located downstream. These interactions have two main consequences: they increase structural fatigue and decrease Annual Energy Production (AEP).

During the design phase of a wind farm, the layout can be optimized to minimize wake losses, usually with the aid of engineering wake models (Shakoor et al., 2016; Cao et al., 2022), while accounting for the local wind rose and site-specific constraints. Unfortunately, wake losses usually cannot be completely mitigated by layout optimization alone. This limitation has motivated the development of wind farm control strategies, which shift the objective from maximizing the power of each turbine individually ("greedy" control) to maximizing the total farm output (Fleming et al., 2014; Munters and Meyers, 2018; Meyers et al., 2022).

Among the control concepts explored in recent years, two main categories have emerged: axial induction control and yaw-based control. In the latter, selected turbines are intentionally yaw-misaligned relative to the incoming wind direction. This generates a lateral thrust component that deflects their wakes away from downstream turbines, a concept known as wake steering control. This kind of strategy can be conveniently implemented in an open-loop manner, using a look-up table (LUT) of optimal yaw settings, usually defined as a function of the free-stream wind speed and direction mainly. Both computational (Gebraad et al., 2016; Vollmer et al., 2016; Fleming et al., 2018) and experimental studies (Campagnolo et al., 2016, 2020) have proven the strategy to successfully enhance the total farm energy yield. Such potential was also confirmed during field campaigns (Fleming et al., 2017, 2019; Doekemeijer et al., 2021; Simley et al., 2021, 2022; Pena Martinez and Coussy, 2024), although with an appreciable uncertainty, mostly resulting from sensors finite accuracy and uncontrolled wind conditions.

The generation of the LUT of yaw commands typically relies both on engineering wake models, to ensure a computational affordability (Gebraad et al., 2016), and on idealized incident flows, assumed steady, unidirectional, and horizontally homogeneous if not uniform. In the field, wind farm flows can be much more complex. Primarily, the atmospheric stability, as well as the related veer, can significantly influence control performance (Vollmer et al., 2016; Fleming et al., 2019; Simley et al., 2022). Moreover, turbulence induces unsteadiness in both wind speed and direction, posing challenges for controller design (Bossanyi, 2018; Campagnolo et al., 2020). Another practical constraint arises from turbine yaw control: limited actuation rates and travel ranges can restrict the achievable yaw misalignments, potentially preventing turbines from reaching their target positions before control updates (Mittelmeier and Kühn, 2018; Simley et al., 2020).

To improve the robustness of wake steering control, several studies have introduced 'Optimization Under Uncertainty' (OUU) frameworks. First, accounting for uncertainty in the achieved yaw misalignments showed to better secure the power gain compared to the deterministic optimization (Quick et al., 2017). Subsequently, the dynamic nature of the wind direction, due to the incoming turbulence structures, was addressed in (Rott et al., 2018). A zero-mean Gaussian distribution was proposed to model the resulting discrepancies between the measured and true wind direction, with the standard deviation σ as a way to reflect the turbulence intensity. For each wind direction of interest, this formulation finally optimizes yaw commands over a discretized set of wind directions, weighted according to this Gaussian distribution. Applied to a nine-turbine test farm, the

https://doi.org/10.5194/wes-2026-37
Preprint. Discussion started: 17 February 2026
© Author(s) 2026. CC BY 4.0 License.

eawe european academy of wind energy
Open Access WIND ENERGY SCIENCE DISCUSSIONS

method consistently outperformed deterministic optimization. Later, a third framework was proposed (Simley et al., 2020) to combine the two above kinds of uncertainty. Considering stochastic wind direction signals derived from LES and met-mast spectra, the enhanced optimization process showed again to improve the control performance, especially for large turbine spacings. Interestingly, the wind direction variability emerged as the dominant uncertainty source.

While these improved optimization approaches make open-loop wake steering more reliable, they still rely upon engineering wake models to reduce the return time. Such models often exhibit limitations in complex flow conditions, especially where multiple full or partial wake interactions occur, situations which are critical for wake steering control (Doekemeijer et al., 2022; Bay et al., 2023). Model-based uncertainties may thus arise from parameter tuning and simplifications (Zhang and Zhao, 2020). Continued calibration and validation using field data (Van Beek et al., 2021; Doekemeijer et al., 2022; Göçmen et al., 2022; van Binsbergen et al., 2024), complemented by detailed comparisons with high-fidelity methods such as LES (Gebraad et al., 2016; Fleming et al., 2018; Doekemeijer et al., 2020; Göçmen et al., 2022; Quick et al., 2024; Steiner et al., 2025), thus remain essential.

Moreover, the modeling of the absolute wind direction uncertainty from previous studies looks incomplete. A zero-mean Gaussian distribution does not intrinsically encompass the modeling of a static error in the absolute wind direction, unless such error is also assumed to obey the same kind of distribution (Murcia et al., 2015). This error does not exist as such in greedy turbine control, as a wind direction relative to the nacelle orientation is enough to operate (Mittelmeier and Kühn, 2018). Yet, for wind farm control strategies, which are usually sector-based, the absolute wind direction is required to identify optimum actions. Establishing the absolute wind direction requires a specific calibration procedure, from which the mentioned static error can first arise. A convenient calibration procedure, which does not need extra hardware, can be built from SCADA signals (mean power production ratios, wind speed variability), either analyzed in light of the farm layout (Réthoré et al., 2009) or compared with wake model predictions (Liu et al., 2025). However, sparse SCADA data, wake model assumptions, or complex layouts can introduce a residual bias in the calibration output. Besides, additional drift may occur over time due to sensor degradation (Bromm et al., 2018). Consequently, the measured absolute wind direction may systematically deviate from reality by a few degrees.

Similarly to a recent initiative (Hodgson and Andersen, 2025), the present study thus seeked to quantify the impact of such static errors on the performance of open-loop wake steering control. In addition, the robustness of the control strategy was also assessed with regard to possible inaccuracies in the nacelles orientation. More specifically, this work aimed to address, at least partially, several questions of practical interest: (1) How is the total variation in power output distributed across the turbines in the case of active control? (2) Can the aforementioned errors, which are of a few degrees in practice, lead to a loss of total power instead of a gain, in a typical control application scenario? (3) How to practically assess a power benefit with sufficient reliability ? For those main purposes, a layout of four industrial multi-megawatt wind turbines, organized in a row, was examined using both LES and engineering wake models simulations. The simulated configurations are introduced in Section 2.1, and the optimization procedure used to determine the optimal yaw commands is detailed in Section 2.2. The LES solver and numerical setup are described in Section 2.3 and Section 3, respectively. Simulation results are presented in Section 4, beginning with the validation of LES results against field data for the no-control case. The wake model and LES

https://doi.org/10.5194/wes-2026-37
Preprint. Discussion started: 17 February 2026
© Author(s) 2026. CC BY 4.0 License.

eawe european academy of wind energy
Open Access WIND ENERGY SCIENCE DISCUSSIONS

results are then compared in terms of power production and time-averaged flow fields, and the instantaneous wake meandering obtained with LES is closely analyzed. Finally, Section 5 proposes a final discussion that wraps up all made observations, to suggest improvement pathways for open-loop wake steering control strategies.

2 Configuration and simulations tools

2.1 Layout and configurations

The investigated layout consists of four multi-megawatt industrial wind turbines, labeled T1 to T4, all of an identical design owned by Siemens Gamesa Renewable Energy, which feature a rotor diameter D. This layout is shown in Fig. 1. It matches a subset of a real offshore wind farm, which cannot be revealed for reasons of anonymity. The orientation α of the layout is defined by the alignment direction of turbines T1 and T4, relative to the wind direction, which is aligned with the x-direction of the main reference frame. In all simulations, this orientation was set to $\alpha = \alpha_0 = -2°$. Five configurations, listed in Table 1, have been investigated. They differ in the following ways:

- Whether or not the wake steering farm control strategy is on or off. When off, the yaw command $\gamma_{c,i}$ is set to 0°, for each turbine i.
- The values of the applied yaw command $\gamma_{c,i}$ for turbine i, in case of active control. For each configuration, those are assumed to be optimal for the wind direction $w_d = \alpha_0 + e_d$, given relatively to the layout orientation. The quantity e_d refers to a static bias that may occur in the field when assessing the absolute wind direction. It is worth stressing that this bias is only a concern for the free-stream turbine (T1 in this case), as the LUT of yaw commands is in practice usually accessed considering the wind condition measurements from free-stream turbines only.
- Whether or not there is a signed error e_γ in the positioning of the nacelles, relative to the yaw commands applied. For simplicity's sake, this error is assumed to be identical for all turbines, even though such a scenario would be unlikely in practice. The final orientation of each turbine i is denoted $\gamma_i = \gamma_{c,i} + e_\gamma$, and is defined with respect to the wind direction.

Parameters mentioned above are given in Table 1 for all configurations. To limit the computational cost of the study, all of these simulations have been performed for a unique wind speed U_∞ at hub height z_{hub}, slightly lower than the rated wind speed U_R. Given the fact that the wake steering strategy is mostly relevant for the below-rated regime only, the choice of U_∞ was motivated by the power increase ΔP achievable with the control strategy. Indeed, according to the Gaussian wake model (Bastankhah and Porté-Agel, 2016) and as illustrated in Fig. 2, the power increase is expected to concentrate predominantly in the selected wind speed range. Furthermore, the layout orientation α_0 was selected on purpose to target the maximum power increase. Similarly, the wind direction bias e_d considered in configurations 3 and 5 leads to yaw commands that would allow an approximately identical power increase in case of the opposite layout orientation $\alpha = -\alpha_0$.

https://doi.org/10.5194/wes-2026-37
Preprint. Discussion started: 17 February 2026
© Author(s) 2026. CC BY 4.0 License.

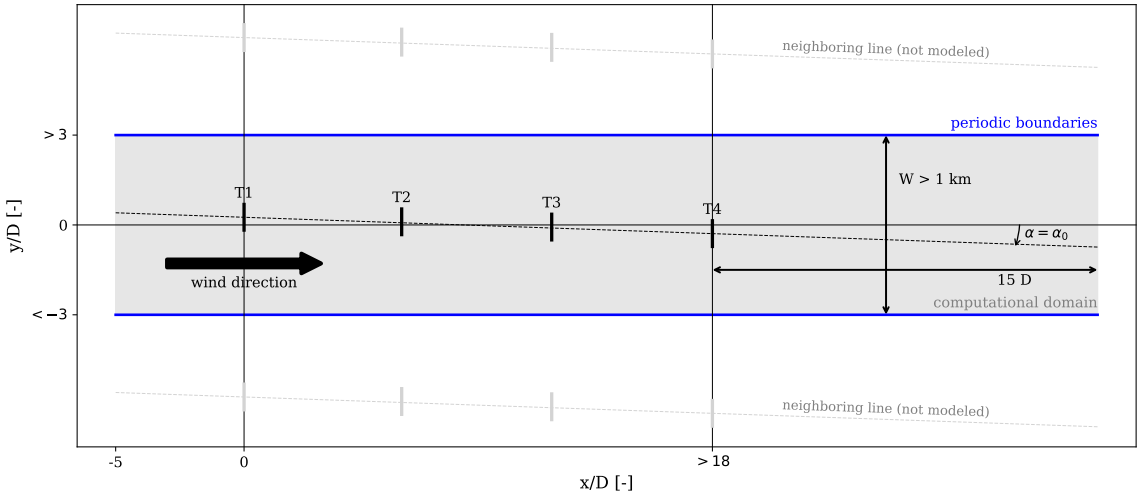

Figure 1. Real 4-turbine layout investigated in this work, viewed from above. The turbines are arranged in a row, which is rotated by $\alpha_0 = -2°$ relative to the wind direction. Exact spacings and dimensions are kept undisclosed to preserve anonymity.

Table 1. Simulated configurations and corresponding parameters.

Config. #	Farm control	e_d	e_γ
1	Off	0	0
2	On	0	0
3	On	4	0
4	On	0	-2
5	On	4	-2

2.2 Wake modeling and model-based optimization

Optimal yaw commands were calculated using the FLORIS (FLow Redirection and Induction in Steady state) library (version 4.2.2) (Gebraad et al., 2016; National Laboratory of the Rockies (NLR), 2024), mainly developed by the National Laboratory of the Rockies (NLR). More specifically, an existing implementation of the OUU approach in FLORIS, as designed in (Rott et al., 2018), was used in this work. To model the dynamic wind direction error, the related 0-centered Gaussian distribution was set with a standard deviation $\sigma = 3°$. This value is consistent with the precursor wind used for all LES simulations (see Section 3.1) and matches the wind direction standard deviation obtained at hub height. Additionally, for each optimized absolute wind direction, the relative wind directions $[-2\sigma, -\sigma, 0, \sigma, 2\sigma]$ were used in the OUU process, with normalized weights. The resulting optimization problem was numerically solved with the Serial-Refine method (Fleming et al., 2022). The optimization problem was formulated and solved for all combinations of the following wake sub-models:

https://doi.org/10.5194/wes-2026-37
Preprint. Discussion started: 17 February 2026
© Author(s) 2026. CC BY 4.0 License.

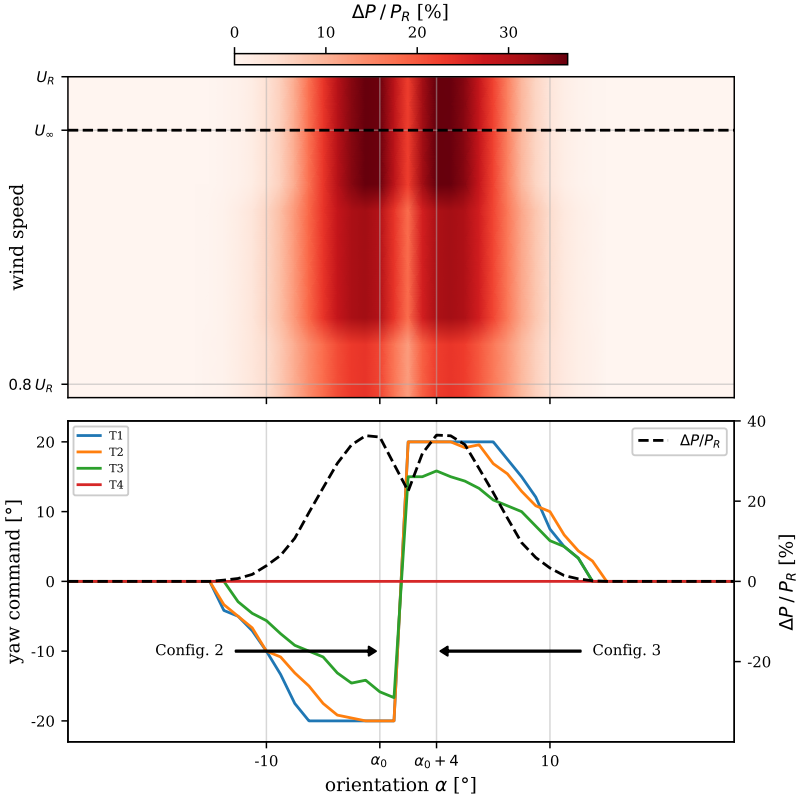

Figure 2. Total power gain (top), given as a fraction of the turbine rated power P_R for a below-rated wind speed range, and optimal yaw commands (bottom) at the target wind speed U_∞. All results have been obtained with the Gaussian wake models (velocity deficit and wake deflection) and the 'sum of squares' wake combination approach.

- **Velocity deficit model**: Gaussian (Bastankhah and Porté-Agel, 2016; Niayifar and Porté-Agel, 2016), Cumulative Curl (Bay et al., 2023), Jensen (Jensen, 1983)
- **Deflection model**: Gaussian (Bastankhah and Porté-Agel, 2016; King et al., 2021), Jimenez (Jiménez et al., 2010)
- **Wake Combination model**: linear, 'sum of squares' (see (National Laboratory of the Rockies (NLR), 2025))
- **Added turbulence model**: Crespo-Hernandez (Crespo and Hernandez, 1996) (superposition approach from (Niayifar and Porté-Agel, 2016))

In each sub-model, the default parameters were used, which are defined according to the literature, in a built-in example from the FLORIS library. For illustrative purposes, the yaw commands obtained with the Gaussian wake models and the sum-of-squares combination model are given in Fig. 2, as a function of the relative wind direction α and for the wind speed U_∞. A sudden jump of the yaw commands can be observed as α becomes positive, where the wakes switch from a left to right

https://doi.org/10.5194/wes-2026-37
Preprint. Discussion started: 17 February 2026
© Author(s) 2026. CC BY 4.0 License.

eawe european academy of wind energy
Open Access WIND ENERGY SCIENCE DISCUSSIONS

partial impingement on the downstream turbines. As a result, the optimal yaw commands for $e_d = 0°$ (configs. 2 and 4) and for $e_d = -4°$ (configs. 3 and 5) are of very similar magnitude but their sign differ.

To unify the optimization results and thus factor in wake models diversity, the applied yaw command sets in all LES simulations, then possibly combined with a nacelle positioning error, were taken as the average of the sets individually given by each combination of sub-models. Yet, the FLORIS simulation results discussed in Section 4, although based on the same average yaw commands, were all obtained with the Gaussian wake models and the 'sum of squares' wake combination method only, given the wide use of this approach in the wind energy community and for the sake of clarity. To further highlight the differences in effective yaw misalignments, the static orientation of each turbine is given in Fig. 3 for all configurations. The corresponding yaw misalignment angles are given in Table 2.

Table 2. Yaw misalignment applied for each turbine, in each configuration.

	$\gamma_{c,i} + e_\gamma$ [°]			
Config. #	T1	T2	T3	T4
1	0	0	0	0
2	-19.8	-19	-15.5	0
3	19.4	18.3	16	0
4	-21.8	-21	-17.5	-2
5	17.4	16.3	14	-2

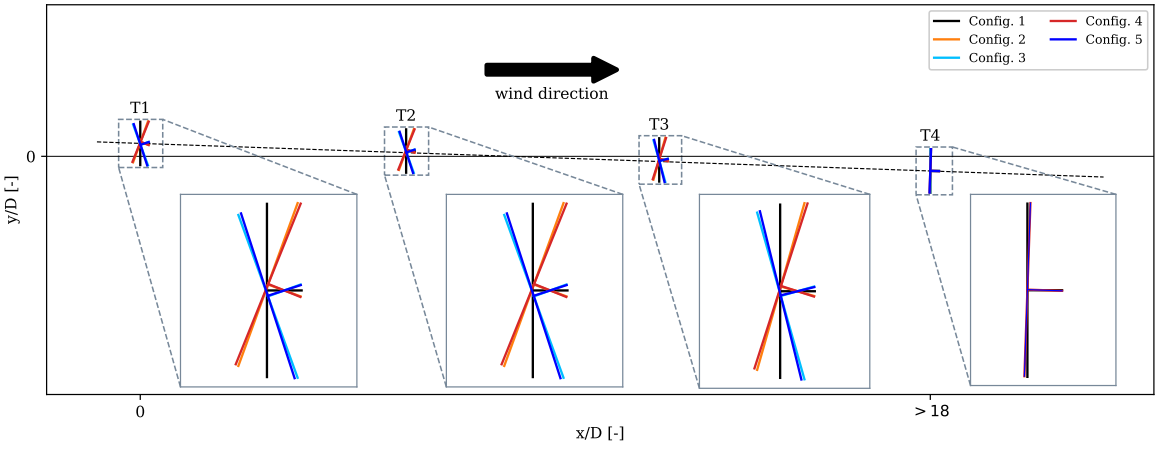

Figure 3. Orientation of the wind turbines in all studied configurations. Exact spacings between turbines are kept undisclosed to preserve anonymity.

https://doi.org/10.5194/wes-2026-37
Preprint. Discussion started: 17 February 2026
© Author(s) 2026. CC BY 4.0 License.

eawe european academy of wind energy
Open Access WIND ENERGY SCIENCE DISCUSSIONS

2.3 LES solver

The case of a truly neutral atmospheric boundary layer (ABL) was considered in all LES simulations carried out in this work. In this context, and noting $\tilde{.}$ the implicit spatial filtering, the simulated ABL obeys the filtered Navier-Stokes equations for incompressible flows, written as:

$$\boldsymbol{\nabla} \cdot \tilde{\boldsymbol{u}} = 0, \tag{1}$$

$$\frac{\partial \tilde{\boldsymbol{u}}}{\partial t} + (\tilde{\boldsymbol{u}} \cdot \boldsymbol{\nabla})\, \tilde{\boldsymbol{u}} = -\boldsymbol{\nabla} \tilde{p} + \nu \boldsymbol{\nabla}^2 \tilde{\boldsymbol{u}} + \boldsymbol{\nabla} \cdot \boldsymbol{\tau}_{\mathrm{SGS}} + \boldsymbol{f}, \tag{2}$$

where ν is the constant kinematic viscosity, $\tilde{p}$ is the pressure divided by the air density ρ, and $\boldsymbol{f}$ refers to a body acceleration term which typically encompasses the forcing terms. The subgrid-scale stress tensor is noted $\boldsymbol{\tau}_{\mathrm{SGS}}$ and was assessed with the localized version of the dynamic model of Smagorinsky (Lilly, 1992). In this work, either the standalone library YALES2 (Moureau et al., 2011) or the coupled software YALES2-BHawC (Muller et al., 2024) were used to solve the above equations numerically.

2.3.1 YALES2 library

The YALES2 library contains a set of solvers which are mainly intended for the LES simulations of various flow problems. Most of these solvers rely on a massively parallel node-centered finite volume method, for either structured or unstructured meshes, and are therefore totally suitable for high performance computing systems.

In this work, the solver for incompressible flows at constant density was used to solve Equations (1) and (2). A 4th-order central scheme is used to discretize the equations in space, and the time integration is performed with the 4th-order explicit TFV4A scheme (Kraushaar, 2011), which is a modification of the classic Runge-Kutta scheme of order 4. The time-step size δt is adaptative with respect to a CFL number constraint. The pressure-velocity coupling was addressed with the projection method of Chorin (Chorin, 1968). The resulting Poisson equation for the pressure was solved with an efficient in-house linear solver, based on the deflated preconditioned conjugate gradient (DPCG) method (Malandain et al., 2013).

Furthermore, and in order to model operating wind turbines in the simulated flows, the solver was combined with an implementation (Bénard et al., 2018; Houtin-Mongrolle, 2022) of the actuator line (AL) method (Sørensen and Shen, 2002). Especially, the actual rotor blades were replaced by as many rotating actuator lines. Each line was uniformly discretized with a set of actuator points. The aerodynamic forces acting on each blade were calculated at the actuator points spanwise positions, from airfoil polars conveniently stored in a look-up table. It is worth noting that, for the sake of simplicity, no correction of neither the polars or of the aerodynamic loads were used in this work. The tip losses predicted by the AL method were thus kept unaltered. Similarly, the dynamic stall phenomenon was not factored in. Once calculated, the pointwise aerodynamic forces are projected on the 3D mesh, using the standard isotropic Gaussian-like smearing kernel. Following the approach described in (Stevens et al., 2018), both the nacelle and tower of each turbine were also modeled with two fixed actuator lines.

https://doi.org/10.5194/wes-2026-37
Preprint. Discussion started: 17 February 2026
© Author(s) 2026. CC BY 4.0 License.

eawe european academy of wind energy
Open Access WIND ENERGY SCIENCE DISCUSSIONS

2.3.2 YALES2-BHawC coupling

In order to get a more realistic modeling of the wind turbines in YALES2, the library was recently coupled (Muller et al., 2024) to the aero-servo-elastic solver BHawC (Rubak and Petersen, 2005; Skjoldan, 2011) from Siemens Gamesa Renewable Energy. This software implements a finite-element-based structural solver which allows to model a wind turbine as a set of connected sub-structures (i.e. foundation, tower, nacelle, hub, rotor blade, bearings, etc...), which feature different element types and degrees of freedom. The solver additionally includes a complete emulation of the controller strategy, making the rotor rotation speed and the individual pitch angles intrinsically non-steady.

In its standalone version, BHawC computes the aerodynamic loads acting on the blades using the Blade Element Momentum (BEM) method. This setup allows to run efficiently all the Design Load Cases (DLCs) defined in the standards, to predict deformations and loads. When using the YALES2-BHawC coupling, the aerodynamic loads are instead assessed with YALES2 and the AL method at each time iteration, and then transferred to BHawC. In turn, and still considering the turbine controller emulation, BHawC calculates the resulting movements and deformations of the blades, before feeding those back into YALES2. In essence, this loose coupling thus provides an Elastic Actuator Line (EAL) framework, as well as non-steady operating parameters which update realistically according to the time-varying wind conditions. The framework can be used to simulate several wind turbines at the same time, as done in this work.

3 LES numerical setup

3.1 Precursor simulation

All LES simulations of the configurations from Table 1 were performed using a precursor-successor approach. Especially, a single offline precursor simulation was run to establish a truly neutral atmospheric boundary layer, then used as inflow condition for all successor simulations. The precursor domain is illustrated in Fig. 4, with the instantaneous axial velocity field given in a horizontal and vertical sections. This domain was meshed with an extruded transfinite mesh, featuring a homogeneous and isotropic cell size $\delta_0 = D/16$.

Periodic boundary conditions were applied for the inlet/outlet pair, as well as for the lateral boundaries. A slip condition was applied on the upper boundary, and a wall law ruled the bottom boundary. The wall law derives from the logarithmic vertical wind profile for neutral stability, widely used to describe the mean shear profile of the streamwise velocity in the vertical direction z:

$$u(z) = \frac{u_\tau}{\kappa} \log\left(\frac{z + z_0}{z_0}\right), \tag{3}$$

where the parameters u_τ, $\kappa = 0.41$, and $z_0 = 0.005$m denote the friction velocity, the Von Kármán constant, and the roughness height, respectively. The wall law then defines the shear stress τ_w at the wall as:

$$\tau_w = \rho {u_\tau}^2. \tag{4}$$

https://doi.org/10.5194/wes-2026-37
Preprint. Discussion started: 17 February 2026
© Author(s) 2026. CC BY 4.0 License.

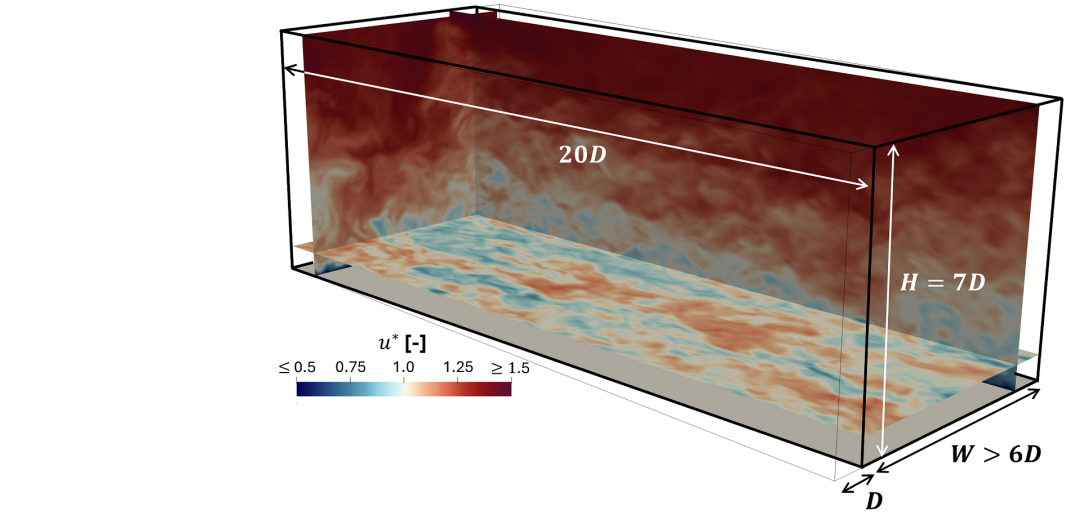

Figure 4. Computational domain used for the precursor simulation. The instantaneous streamwise velocity, obtained after a convergence period of more than 100 flow-through times, is displayed in both a vertical and horizontal planes. The latter is located at hub height.

The shear was calculated for each surface element of the bottom boundary, by retrieving u_τ from Equation (3) at the local nodes defining the first layer of cells. To compensate for the use of an unstructured mesh, which typically leads to a non-homogeneous thickness of this layer of cells, the vertical position of the nodes was spatially filtered with a Gaussian kernel. The same procedure was applied for the local velocity norm. This contributed to denoise the final shear applied on the bottom boundary.

To establish the fluid motion, a constant body acceleration term $f_p = {u_\tau}^2/H$, behaving as a pressure gradient, was added to the streamwise momentum equation. This terms aims to compensate for the theoretical and uniform shear stress at the bottom wall. Yet, because the effective shear is expected to differ slightly from the theoretical one, a supplementary source term f_c, defined following the 'pressure controller' approach (Stipa et al., 2024), was added to ensure a wind speed U_∞ at hub height, on average in space.

We emphasize that the domain had a parallelepiped geometry. This was used to avoid the appearance of stationary longitudinal vortices, which would lead to non-physical gradient of the mean velocity field in the lateral direction, also referred as 'streaks' in the literature. This domain shape coupled to the periodic boundary conditions allowed the turbulent structures to slowly translate laterally without gaining a lateral velocity component. Nevertheless, the domain shape was chosen almost rectangular, to avoid skewing the flow artificially. A $1D$ lateral translation of the outlet showed to be appropriate in this case.

The flow was converged during more than 100 flow-through times, defined from the target velocity U_∞ at hub height, which proved sufficient to fully develop the wall shear and to propagate homogeneously the turbulence in the vertical direction. Then, wind boxes were generated by temporally sampling the instantaneous velocity field in a cross-flow plane every 0.4s during 20 additional flow-through times at the wind speed U_∞, in order for the successor simulation workflow to be fully covered. These

https://doi.org/10.5194/wes-2026-37
Preprint. Discussion started: 17 February 2026
© Author(s) 2026. CC BY 4.0 License.

eawe european academy of wind energy
Open Access WIND ENERGY SCIENCE DISCUSSIONS

boxes were injected into the successor computational domain for all studied configurations. Considering the wind box thus generated for the streamwise velocity u, we obtained the time-averaged velocity $\langle u \rangle_T / U_\infty$ and resolved turbulence intensity
230 $\sigma(u)_T / U_\infty$ fields depicted in Fig. 5. The turbulence intensity was found close to 6.5% at hub height, a value often met in the offshore domain.

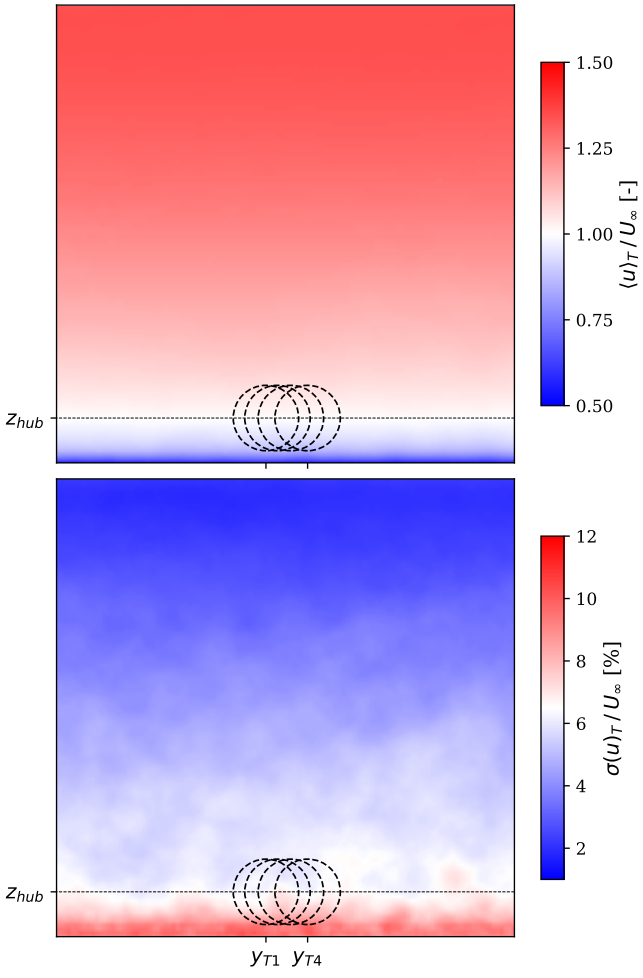

Figure 5. Time-averaged streamwise velocity field $\langle u \rangle_T / U_\infty$ (top) and turbulence intensity $\sigma(u)_T / U_\infty$ (bottom), as obtained in a vertical plane within the precursor simulation. The statistics were collected over a period T of around 20 flow-through times at the wind speed U_∞.

3.2 Successor simulations

Contrary to the precursor domain, the successor computational domain was shaped as a fully rectangular box for simplicity. In the streamwise direction, this domain extended from $5D$ upstream of the leading turbine T1, up to $15D$ downstream of the
235 last turbine T4. As for the precursor domain, the domain height was set to $H = 7D$, and the lateral extent to $W > 6D$ to match

https://doi.org/10.5194/wes-2026-37
Preprint. Discussion started: 17 February 2026
© Author(s) 2026. CC BY 4.0 License.

eawe european academy of wind energy
Open Access WIND ENERGY SCIENCE DISCUSSIONS

the mean spacing observed in the field between the actual rows of turbines. Therefore, and despite the misalignment α_0 of the layout with respect to the wind direction, periodic boundary conditions were applied on the lateral boundaries, as a simple way to factor in the presence of neighboring rows of turbines (cf. Fig. 1).

All successor simulations were performed using a multi-step workflow, derived from the one described in (Patel et al., 2024). This workflow, in essence, allows to successively propagate the precursor inflow in the successor domain and generate a suitable mesh with the MMG library (Dapogny et al., 2014), to finally collect the flow and turbine operation statistics, all automatically. The final cell size mappings thus obtained are represented in Fig. 6, for configurations 2 and 3 of Table 1. As one can observe, they are very representative of the wake deflections achieved in each case. The cell size was deliberately coarsened to $\delta = D/8$ in the region preceding the outlet, to damp the leaving turbulence structures. All final meshes were counting more than 140M cells. To lower the simulation cost, the YALES2-BHawC coupling was only activated in last step of the workflow, using the final meshes. The turbine response was then initialized, and the resulting flow propagated, during one flow-through time at the wind speed U_∞. Most of the results and time statistics reported in Section 4 were finally collected over a period $T_s = 1200$ s.

Nonetheless, to characterize further the simulated time-averaged power productions and power gains, a non-parametric bootstrap procedure was additionally employed. Specifically, the 1200 s time series were divided into consecutive non-overlapping segments of 60 s, matching the samples duration sometimes selected in wake-steering field experiments (Simley et al., 2021). From the segment-averaged values, subsets of $n = 5$ samples were considered for the statistical analysis, in order to represent a wind condition bin (in terms of wind speed, wind direction and turbulence intensity) for which the amount of collected data during a field campaign would be very low. The subsets were drawn 5000 times with replacement, to generate an empirical distribution of the mean values. The associated uncertainty bounds were here assessed using the bootstrap standard deviation. This choice was made to provide a direct measure of variability, which in this context is more appropriate than a strict coverage-based confidence interval, given the limited effective sample size and the objective of comparing relative trends between configurations.

The cumulative computational cost of the workflow, was on average of 100k CPU hours per configuration, with the workflow final step accounting for more than 80% of this cost. The significant computational cost of YALES2-BHawC is caused in part by a fixed time-step $\Delta t = 0.02$ s, which was required on BHawC side to ensure the numerical stability. All final meshes were distributed on 508 processors to run YALES2. A separate BHawC instance was additionally running on a single core for each turbine, leading the coupled-code to run on 512 CPU cores in total. All simulations were run on the Joliot-Curie supercomputer from the CEA's TGCC facilities in France, using the AMD Irene ROME partition.

4 Results

4.1 Power production

Since the primary objective of the wake steering control strategy is to maximize the energy efficiency of a wind farm, the results obtained in terms of power production are presented first, both at the wind turbine and cluster levels.

https://doi.org/10.5194/wes-2026-37
Preprint. Discussion started: 17 February 2026
© Author(s) 2026. CC BY 4.0 License.

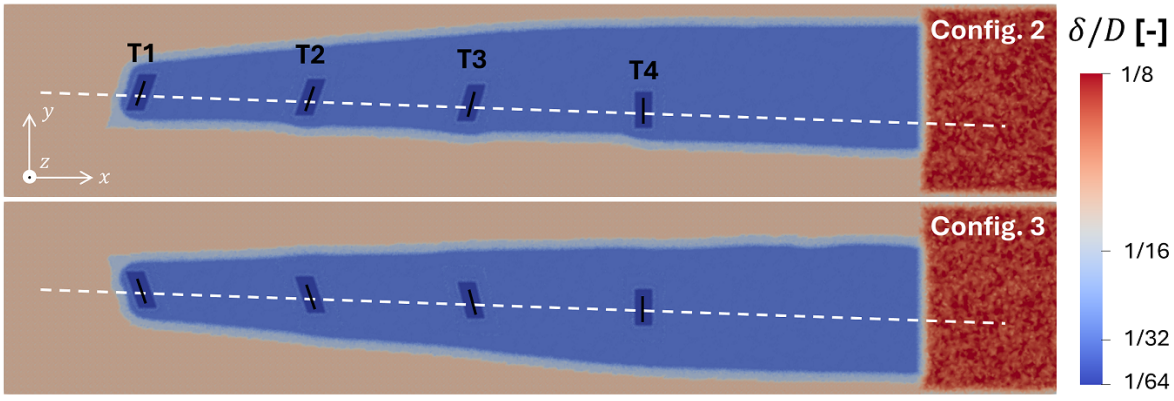

Figure 6. Cell size mappings at hub height, in the final meshes obtained for configurations 2 and 3. The cell-size is locally calculated at each node, considering the length of the edges connecting a node to the neighboring ones.

4.1.1 Power ratios

The time-averaged power produced $\langle P^*_{i,j} \rangle_T$ by turbine T_i in configuration j is defined as follows:

$$\langle P^*_{i,j} \rangle_T = \langle P_{i,j} \rangle_T / P_{\text{REF}}, \tag{5}$$

where T refers to the time-averaging period. We also define the reference power P_{REF} as the power $\langle P_{1,1} \rangle_{T=T_s}$ obtained with YALES2-BHawC. The above quantities, also referred to as 'power ratios', are given in Fig. 7 for all investigated configurations.

In the baseline case (i.e. configuration 1), the power ratios were also assessed from 10-minute SCADA samples. The raw SCADA data were post-processed with a set of filtering operations ensuring the normal and simultaneous operation of all turbines within the cluster being studied, and as well of the nearest neighboring turbines (although not part of the performed simulations). Furthermore, the relevant wind speed and direction are identified from the SCADA data attached to the turbine T1, with tolerances of 0.3 m/s and 3°, respectively. It is worth stressing that the target wind direction used for filtering corresponds to the alignment angle between T1 and T4, which therefore differs by 2° from the simulated wind direction. This approach was preferred considering both the existing uncertainties on the wind direction signal and the high expected sensitivity of the power ratios to the wind direction in this sector. For each timestamp available, the consistency of the measured wind directions was inspected to best represent the statistically homogeneous wind direction from the YALES2-BHawC and FLORIS simulations. In particular, the wind direction measured by each turbine considered in the filtering process could not differ by more than 5° from the median wind direction. Finally, an estimate of the ambient turbulence intensity also allowed to restrict the turbulence intensity range to [4, 9]%. While starting with one year and a half of data, only 9 SCADA timestamps remained valid after the filtering process.

For this first configuration, all $\langle P^*_{1,1} \rangle_T$ ratios obtained with FLORIS or from SCADA data are close to one, indicating both the consistency of the power curve used as input in FLORIS, and the adequate filtering of the SCADA samples in terms of

https://doi.org/10.5194/wes-2026-37
Preprint. Discussion started: 17 February 2026
© Author(s) 2026. CC BY 4.0 License.

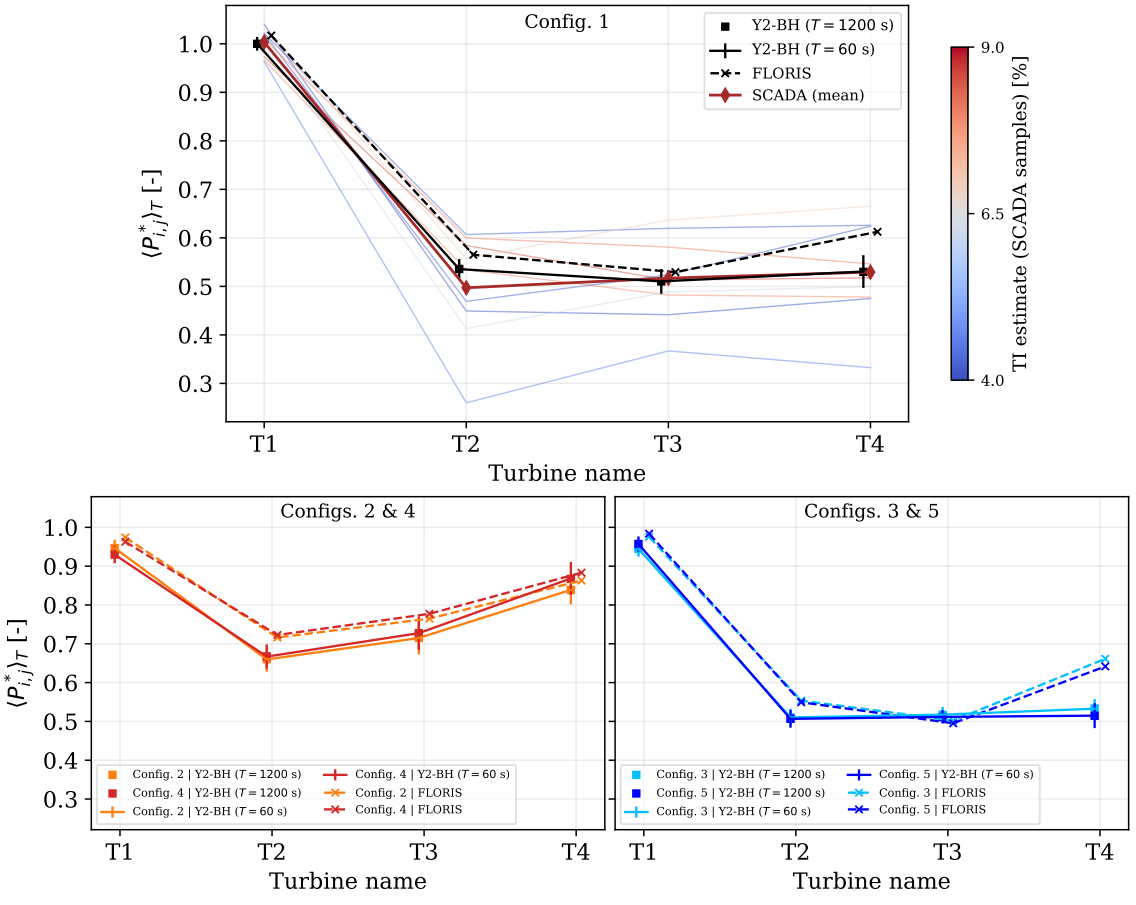

Figure 7. Comparison of the power ratios obtained for 0° yaw misalignments (top), the 'optimum' yaw commands (bottom left), and the 'reversed' yaw commands (bottom right), as obtained with FLORIS and YALES2-BHawC (Y2-BH). In configuration 1, the ratios related to 9 10-minute SCADA samples, deemed valid by the filtering process, are also displayed as thin lines. The color bar is further used to denote the ambient turbulence intensity estimate associated with each sample. The YALES2-BHawC results are obtained either by setting the averaging period to $T = T_s = 1200$ s, or by using bootstrapping with intermediate results averaged on 1-minute sub-periods (i.e. $T = 60$ s). In the latter case, error bars are used to indicate the standard deviation obtained on the depicted values.

https://doi.org/10.5194/wes-2026-37
Preprint. Discussion started: 17 February 2026
© Author(s) 2026. CC BY 4.0 License.

eawe european academy of wind energy
Open Access WIND ENERGY SCIENCE DISCUSSIONS

free-stream wind speed. As one would expect, an overall increase of the power ratios for the downstream turbines is observed for higher ambient turbulence intensities. From this regard, and given the rotation α_0 of the layout in the simulations, the YALES2-BHawC results appear consistent. The results obtained with the wake models are also in a good agreement with the SCADA data and the LES results, at least up to the turbine T3. Yet, the selected modeling setup tends to over-predict the power production of the waked turbines.

For configurations 2 and 4, involving the use of the 'optimal' yaw commands, both the LES and engineering wake models results clearly emphasize the effectiveness of the wake steering control strategy. Indeed, despite T1 producing less power as a result of its yaw misalignment while facing the same inflow, the power ratios obtained for the three downstream turbines are significantly increased with respect to the baseline case. However, there are still noticeable differences between the predictions of the simulation tools. The ratios predicted with the wake models are higher on turbines T2 and T3. This gap is then closing on the most downstream turbine, suggesting that the wake deflection achieved, helped by the secondary wake steering mechanism (Fleming et al., 2018) resulting from the lateral induced velocity, is stronger in the LES simulations. This may be correlated to the periodic boundary conditions used in YALES2 on the lateral boundaries. To a certain extent, the simulated flow thus includes lateral velocities that the neighboring turbines would induce by being yawed identically. However, this may also result in part from the turbine row orientation, which would favor the propagation of the wakes on a preferred side of the row. Finally, the nacelle positioning error in configuration 4, which was expected to be beneficial to the control strategy in this case, does lead to higher power ratios in both the LES and wake models results.

The results obtained for configurations 3 and 5 stress the high sensitivity of the wake steering control strategy to the measured wind direction. An error of only 4° in the absolute wind direction, made on purpose in the most unfavorable direction, leads to power ratios that are very similar to configuration 1, if not lower. Both the LES and the wake models agree on this trend, although discrepancies can be observed. Indeed the power ratios for the turbine T4 obtained with the wake models show to be noticeably higher in comparison to the LES results, even in configuration 5 despite the unfavorable nacelle positioning error.

All configurations considered, the YALES2-BHawC results obtained with bootstrapping show the variability of the mean power ratios to increase with the downstream position, which is consistent with the wake-added turbulence and wake meandering effect. Interestingly, this variability is of higher amplitude than the differences in power ratios resulting from the nacelle positioning errors, indicating that those only have marginal effect on the results and would thus be challenging to properly detect in the field.

4.1.2 Power gains

One can also consider the previous results in terms of instantaneous and time-averaged power gains, first at the level of each turbine. For a turbine i in configuration j, the gain $G^*_{i,j}$ was formulated with respect to the power produced by the turbine T1

https://doi.org/10.5194/wes-2026-37
Preprint. Discussion started: 17 February 2026
© Author(s) 2026. CC BY 4.0 License.

in configuration 1:

$$G^*_{i,j} = \frac{P_{i,j} - P_{i,1}}{\langle P_{1,1} \rangle_{T=T_s}}, \tag{6}$$

$$\langle G^*_{i,j} \rangle_T = \frac{\langle P_{i,j} - P_{i,1} \rangle_T}{\langle P_{1,1} \rangle_{T=T_s}}, \tag{7}$$

where the duration T was again set either to T_s or to one minute for the LES results. The obtained results are given in for all configurations applying non-zero yaw commands.

Figure 8. Comparison of the time-averaged (left) and instantaneous (right) power gains/losses for each turbine, given as a fraction of the power $\langle P_{1,1} \rangle_{T=T_s}$. The time-averaged results are given both for FLORIS and YALES2-BHawC. For the latter, results are obtained either by setting the averaging period to $T = T_s = 1200$ s, or by using bootstrapping with intermediate results averaged on 1-minute sub-periods (i.e. $T = 60$ s). In the second case, error bars are used to indicate the standard deviation obtained on the mean values.

We first examine the $\langle G^*_{i,j} \rangle_T$ gains, for which the LES and wake model results can be compared. Those gains are depicted in Fig. 8 (left part). Overall, we observe a good agreement between the wake models and YALES2-BHawC predictions for

https://doi.org/10.5194/wes-2026-37
Preprint. Discussion started: 17 February 2026
© Author(s) 2026. CC BY 4.0 License.

eawe european academy of wind energy
Open Access WIND ENERGY SCIENCE DISCUSSIONS

all configurations with active farm control, even though significant differences have been highlighted in the power ratios. This illustrates that a good prediction of a power gain with the wake models remains feasible even though the power production assessments may not be totally accurate. In configurations 2 and 4, the wake steering strategy shows to be more and more effective with respect to the downstream distance to T1. This trend is even more pronounced in the LES results. Regardless, it is worth noticing that the overall gain is therefore mostly concentrated on the last two turbines. This simple observation is of great importance when it comes to deploy the wake steering strategy in a real wind farm. With the classical open-loop approach, based on accessing a LUT of yaw commands with the free-stream wind conditions, the real background flow field will need to be homogeneous and propagate straight up to the location of the turbine T3 at least, in order to get a significant gain. Depending on the streamwise spacing between turbines, this may be challenging to satisfy due to veer and meso-scale effects, likely to skew and/or curve the wakes. In such scenarios, the yaw commands from the LUT may no longer be optimal, especially for the most downstream turbines. Still, in this particular wind speed and turbulence intensity case, a positive global gain may already be achieved by considering the two first turbines only during the optimization. For the configurations 3 and 5, involving the non-optimal yaw commands, both simulation tools mostly predict power losses, although a few-percent power increase is predicted by the wake models on turbine T4. Still, considering the YALES2-BHawC results obtained with bootstrapping, measuring this gain in practice may not be totally unlikely. As observed for the power ratios, the bootstrapping procedure also shows the variability of the turbine power gains to increase with the downstream distance.

For all optimized configurations, we also note that the power loss on turbine T1 is slightly underestimated in FLORIS in all configurations, which is further illustrated on Fig. 9. The power produced by a turbine yawed with an angle γ is typically approximated with a 'cosine loss' model:

$$P_\gamma(u_{\text{REWS}}) = P_{\gamma=0}(u_{\text{REWS}})\cos(\gamma)^{p_P}, \tag{8}$$

where $P_{\gamma=0}$ is the power produced by the turbine when facing exactly the wind, and p_P is the loss exponent factor. FLORIS sets $p_P = 1.88$ as default value for all turbine models, a value aligned with the original litterature (Gebraad et al., 2016). Yet, to ensure the applicability of the model even with a rotor effective wind speed (REWS) u_{REWS} that would be above-rated in the rotor plane, FLORIS rather implements the cosine loss model as:

$$P_\gamma(u_{\text{REWS}}) = P_{\gamma=0}\left(u_{\text{REWS}}\cos(\gamma)^{p_P/3}\right). \tag{9}$$

With the latter implementation, and according to the LES results, a $p_P \sim 2.4$ should rather be selected. Nevertheless, implementing this revised value in FLORIS for verification purposes only very moderately closed the gap between the LES and wake models results in the configurations 2 to 5, leaving all results trends discussed in this work unchanged. The value $p_P = 1.88$ was therefore kept in FLORIS.

Regarding the instantaneous gains $G^*_{i,j}$ obtained with LES, they are also shown in Fig. 8 (right part) for the time period T_s. In configurations 2 and 4, where the optimal yaw commands are applied, one can see that the gains are positive almost continuously for all the turbines but the leading one. This suggests that the meandering effects in both these configurations and the baseline one cannot lead to significant incidental power losses on a long period, at least for such idealized wind conditions.

https://doi.org/10.5194/wes-2026-37
Preprint. Discussion started: 17 February 2026
© Author(s) 2026. CC BY 4.0 License.

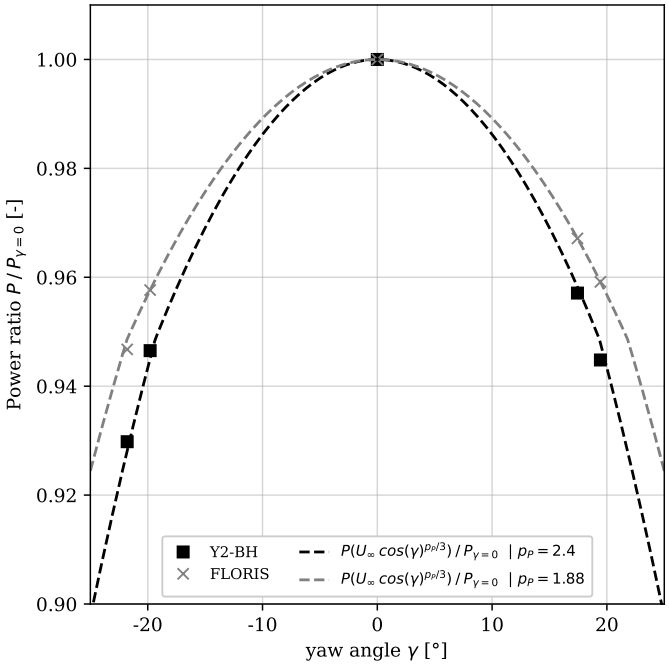

Figure 9. Power ratios for the turbine T1, as a function of the applied yaw misalignment γ and with respect to the non-yawed case, based on the FLORIS and YALES2-BHawC simulations. The results are fitted with the empirical cosine loss model from Equation (9), highlighting a discrepancy in the loss exponent factors p_P.

Conversely, the configurations 3 and 5 show power deltas which are nearly equally distributed between negative and positive. Actually, significant power gains can still be achieved temporarily on the turbine T3 and T4, but power losses of similar magnitude are then set against it.

The instantaneous and time-averaged power gains at the cluster level are shown in Fig. 10 and respectively defined for each configuration j as:

$$G_j^* = \frac{\sum_i (P_{i,j} - P_{i,1})}{\sum_i \langle P_{i,1} \rangle_{T=T_s}}, \tag{10}$$

$$\langle G_j^* \rangle_T = \frac{\sum_i \langle P_{i,j} - P_{i,1} \rangle_T}{\sum_i \langle P_{i,1} \rangle_{T=T_s}}. \tag{11}$$

One can observe that FLORIS and YALES2-BHawC provide very close results for the time-averaged gains $\langle G_j^* \rangle_T$, especially in light of the variability in the YALES2-BHawC results, assessed with bootstrapping. As it matters, it should be noted that this variability is very similar in all configurations. The results further stress the high sensitivity of the wake steering control strategy to the absolute wind direction measured in the field. Indeed, a total power increase of more than 20% can be unlocked for the selected wind conditions and layout orientation. Nevertheless, a 4°-error in the absolute wind direction measurement is enough to turn this benefit into slight power losses.

https://doi.org/10.5194/wes-2026-37
Preprint. Discussion started: 17 February 2026
© Author(s) 2026. CC BY 4.0 License.

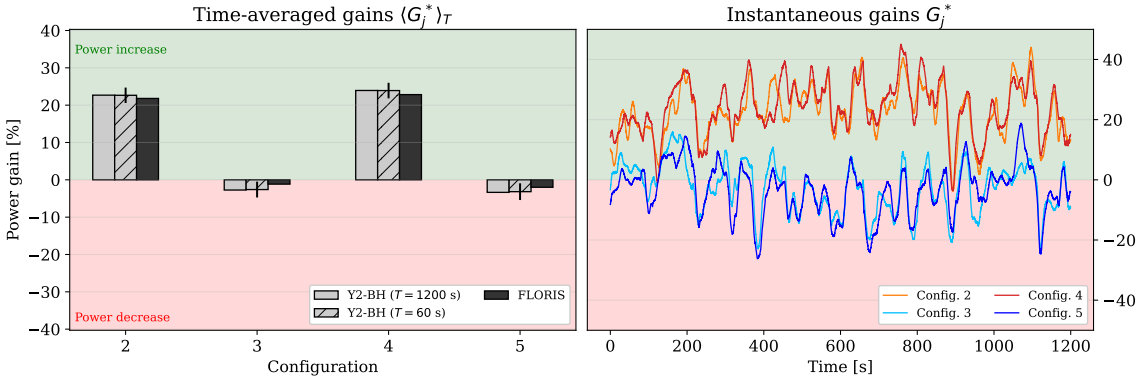

Figure 10. Comparison of the time-averaged (left) and instantaneous (right) power gains/losses at the farm level. The time-averaged results are given both for FLORIS and YALES2-BHawC. For the latter, results are obtained either by considering the full time period $T_s = 1200$ s as the averaging period T, or by using bootstrapping with intermediate results averaged on 1-minute sub-periods (i.e. $T = 60$ s). In the second case, error bars are used to indicate the standard deviation obtained on the mean values.

As for the instantaneous gains G_j^*, displayed also for the time period T_s, they first highlight that a 2° nacelle positioning error, previously shown to impact only marginally the time-averaged results, can still lead the total power production to vary noticeably locally in time. The time series further emphasize a low-frequency oscillation in time, showing a period of approximately 100 s, which was also discernible in the instantaneous gains obtained for the turbine T4. To explore this further, a Discrete Fourier Transform (DFT) was applied on each of these signals, using the Fast Fourier Transform (FFT) algorithm. The resulting spectra are given in Fig. 11, in terms of a Strouhal St number defined as:

$$St = \frac{fD}{U_{\infty,4,1}}, \tag{12}$$

where f is a physical frequency, and $U_{\infty,4,1}$ is the REWS obtained $2.5D$ upstream of the turbine T4 in configuration 1, used as an approximation of the free-stream wind speed seen by this turbine. This choice was made to echo previous results, which have shown the total power variation, when positive, to be mostly achieved with the turbine T4. It can be seen that a significant contribution is attached to the Strouhal number range $[0.1, 0.4]$, which is typical of the meandering induced either by the instability of the annular shear layer on the edge of the wake, or by incoming turbulent eddies having a size close to twice the rotor diameter (Heisel et al., 2018). This suggests that, even when applying appropriate yaw commands, the gain remains largely modulated by the wake meandering amplitude occurring in the baseline case. Consequently, the gain assessment can be complicated in practice, as an adequate time period to compute it, which should contain at least several meandering period, would be likely too long for the wind conditions to stay statistically steady. Albeit not even encompassing a single main period seen in the gains, using 1-minute samples in the field could remain a good trade-off to estimate the gain mean values, provided a sufficient number of samples can be collected for both the baseline and optimized operation modes. The bootstrap procedure applied with the YALES2-BHawC results indeed showed the variability on the mean gains to remain rather small with only 5 1-minute samples for each operation mode.

https://doi.org/10.5194/wes-2026-37
Preprint. Discussion started: 17 February 2026
© Author(s) 2026. CC BY 4.0 License.

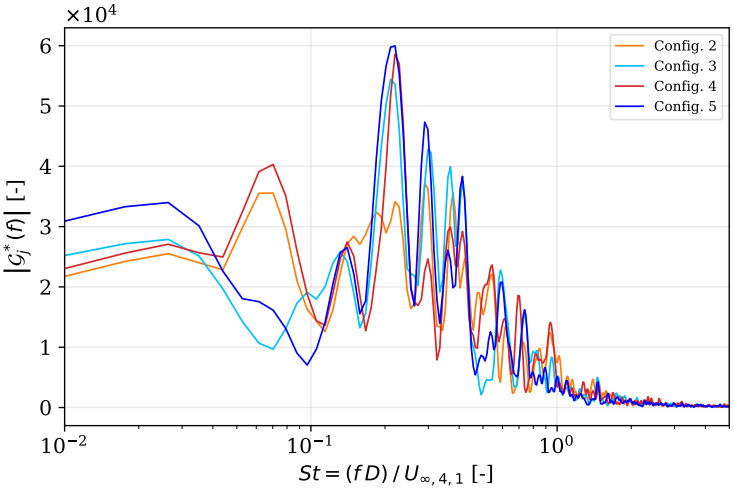

Figure 11. Comparison of the farm-level power gains spectra for configurations 2 to 5. In each case, the Strouhal number used for the frequency axis is defined based on the time-averaged rotor effective wind speed measured 2.5D upstream of the turbine T4, in configuration 1.

4.2 Farm flows

This section presents the wind farm flows in more depth, as simulated with both YALES2-BHawC and FLORIS, with the aim of further characterizing the previous observations made for the power production. A comparison of the time-averaged flow fields obtained for several configurations is first introduced, and discrepancies between the LES and wake model results are analyzed. A special focus is then made on the LES results, to comment the instantaneous flow fields and quantify the wake meandering effect in particular.

4.2.1 Time-averaged flow fields

The LES velocity fields, time-averaged over $T_s = 1200$ s, are depicted in Fig. 12 at hub height for the configurations 1 to 3. A very straight propagation of the wakes is observed in the baseline case. This further indicates that the precursor inflow is, on average, statistically homogeneous in the lateral direction, thus preventing any non-physical deflections of the wakes in the absence of yaw commands. The wakes show to impinge on the downstream turbines almost entirely. In this regard, the configuration 3 is very similar, although wakes impinge predominantly the right side of the downstream rotors. Conversely, the yaw commands applied in configuration 2 result in steering the wake effectively, that is away from the the downstream turbines. Consequence of the yaw commands, a clear lateral velocity is induced in configurations 2 and 3, which tends to amplify as the flow progresses downstream. Especially, this lateral velocity persists downstream of the last turbine T4, although this turbine is not misaligned with respect to the free-stream wind direction. The local wind direction, altered by the induced lateral velocity, is nonetheless misaligned with this turbine, leading to the well known ‘secondary wake steering’ phenomenon (Fleming et al.,

https://doi.org/10.5194/wes-2026-37
Preprint. Discussion started: 17 February 2026
© Author(s) 2026. CC BY 4.0 License.

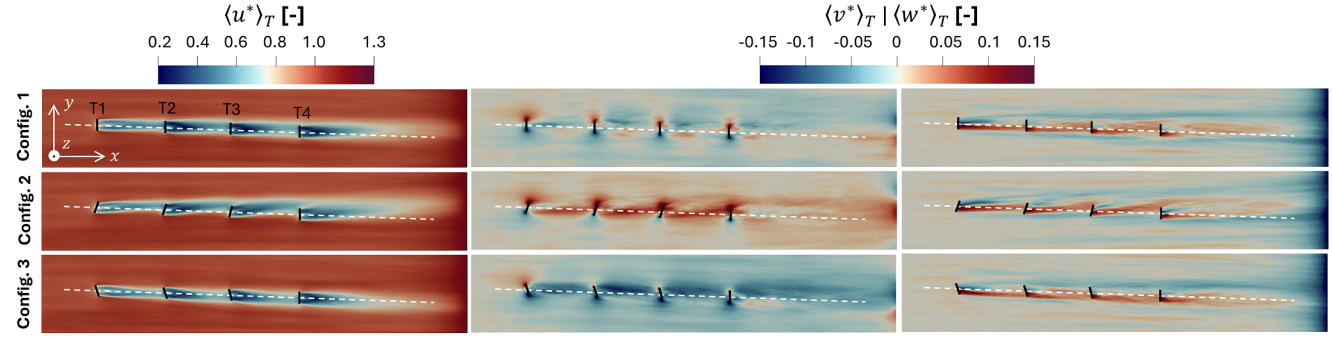

Figure 12. Streamwise (left), lateral (middle) and vertical (right) time-averaged velocity fields obtained with YALES2-BHawC in configurations 1 to 3 (top to bottom), scaled by the target free-stream velocity U_∞. These fields are displayed on a horizontal slice at hub height. The time averaging was performed over the time period $T_s = 1200$ s.

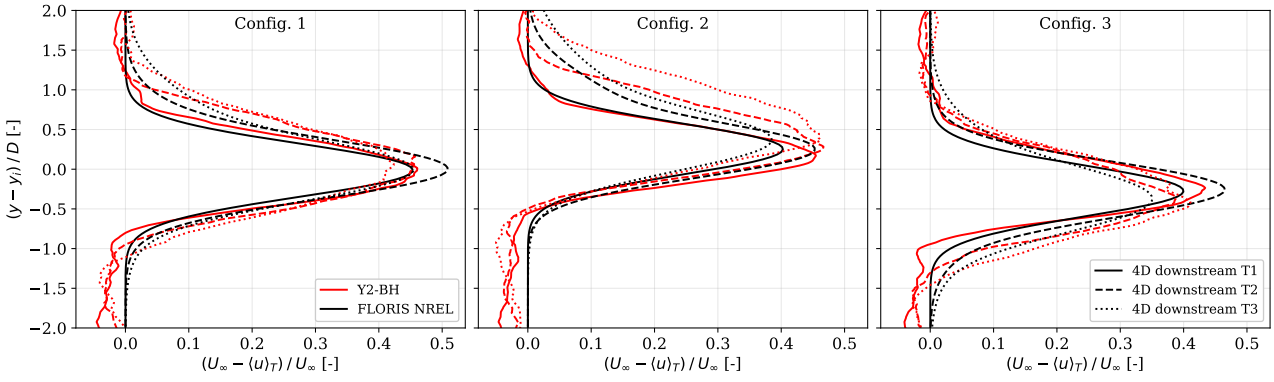

Figure 13. Comparison of the time-averaged streamwise velocity deficits obtained at hub height with YALES2-BHawC and FLORIS in configurations 1 to 3 (left to right), 4 diameters downstream the turbines T1, T2 and T3. The deficits are plotted in the lateral direction, whose origin is given relatively to each rotor center position. For the YALES2-BHawC results, the time averaging was performed over the time period $T_s = 1200$ s.

The time-averaged streamwise velocity deficits, obtained with YALES2-BHawC and FLORIS in configurations 1 to 3, are further compared at hub height in Fig. 13. The deficits were assessed in the lateral direction, 4 diameters downstream the first 3 turbines of the layout. For the baseline configuration, the deficits obtained compare reasonably well overall, with a very good

https://doi.org/10.5194/wes-2026-37
Preprint. Discussion started: 17 February 2026
© Author(s) 2026. CC BY 4.0 License.

match for the deficit behind the turbine T1 in particular. Still, the wake model shows to over-predict the maximum velocity deficit by almost 10% behind the turbines T2 and T3. Although the results are considered at hub height only, the velocity deficits are consistently wider in the LES results. As one may expect, the results in configuration 3 are similar, although the trends from configuration 1 do not confirm entirely. Downstream the turbine T3, the velocity deficit in YALES2-BHawC is wider and stronger, while the wake model predicts a 20% stronger maximum velocity deficit downstream the turbine T2. Considering the lateral deflection of the velocity deficit, the results from both simulation approaches are very well aligned downstream the turbine T1, for which very close values of the thrust were calculated. Finally, meaningful discrepancies are observed in the results from configuration 2. The wake model results are almost identical to those of the configuration 3, except for the wake deflection orientations. On the other hand, the results obtained with YALES2-BHawC show to differ substantially. The velocity deficits from the LES simulation are both deeper and wider, downstream all of the three turbines considered. This asymmetry in the simulation discrepancies for configurations 2 and 3 is additionally illustrated on Fig. 14, by showing the velocity deficit fields at hub height. Similar discrepancies were also reported in (Doekemeijer et al., 2020).

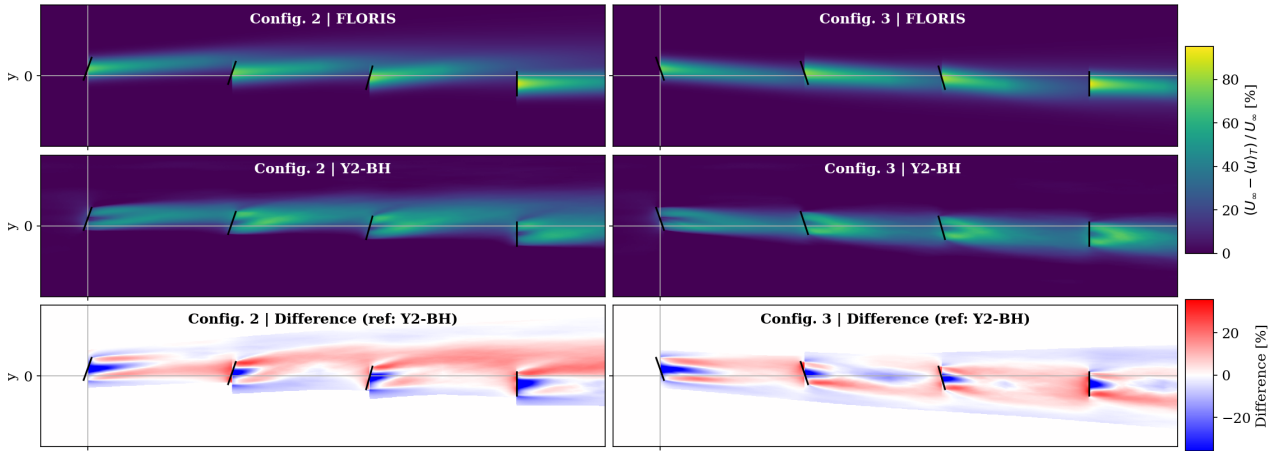

Figure 14. Time-averaged streamwise velocity deficits obtained at hub height with FLORIS (top) and YALES2-BHawC (middle), for the configurations 2 (left) and 3 (right). The discrepancies between the YALES2-BHawC and FLORIS fields are also provided (bottom). For the YALES2-BHawC results, the time averaging was performed over the period $T_s = 1200$ s.

The divergent results given by the wake model in configuration 2 may originate from the wake-added turbulence modeling in FLORIS. Especially, obtaining the effective added turbulence at a rotor location requires to compute overlaps between velocity deficit regions and rotor areas (Niayifar and Porté-Agel, 2016), an approach which may not be appropriate for this partial wake impingement case. To explore further the wake added turbulence, Fig. 15 illustrates the streamwise turbulence intensity at hub height, as resolved with YALES2-BHawC for the configurations 1 to 3. One can again observe clear similarities in configurations 1 and 3 due to the strong wake combinations. Besides, the turbulence generation is roughly symmetric with respect to each rotor rotation axis. The turbulence evolution in configuration 2 differs notably, especially downstream of the

https://doi.org/10.5194/wes-2026-37
Preprint. Discussion started: 17 February 2026
© Author(s) 2026. CC BY 4.0 License.

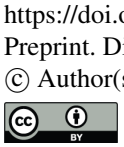

eawe european academy of wind energy
Open Access WIND ENERGY SCIENCE DISCUSSIONS

turbine T2. The partial wake scenario appears to damp the incoming added turbulence, which finally exhibits a fast decay on the left side of the turbine row.

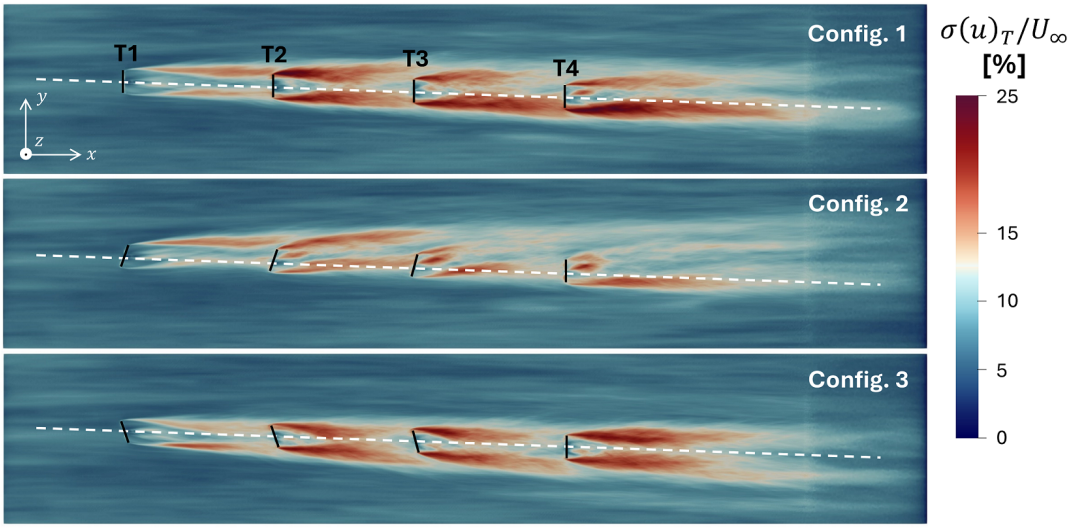

Figure 15. Streamwise turbulence intensity, defined as $\sigma(u)_{T=T_s}/U_\infty$, obtained with YALES2-BHawC on a horizontal slice at hub height, for the configurations 1 to 3 (top to bottom).

4.2.2 Wake deflection and meandering

Three snapshots of the dimensionless streamwise velocity $u^* = u/U_\infty$ at hub height, as computed with YALES2-BHawC for the configurations 1 to 3 respectively, are depicted in Fig. 16. All three snapshots are considered at the exact same physical time to illustrate the identical inflow used for all configurations. All snapshots are providing qualitative insights into the deflection and meandering of the wakes. The latter phenomenon is distinct in configuration 1, and is particularly prominent downstream the turbine T4. The same observation stands for the configuration 3, yet to a lesser extent. On the contrary, the wake deflections are clearly visible and dominating in configuration 2, making the meandering less obvious at first glance.

To quantitatively confirm the previous observations, the instantaneous velocity fields were probed 4 diameters downstream each turbine, in finite planes centered with respect to each rotor center position. The sampling was performed every 0.4 s during the second half of the time period T_s only, to lower the resulting memory footprint, which yet proved to be enough to capture 4 to 5 meandering cycles of the wake generated by the most downstream turbine T4. Considering that several wakes were expected to partially or fully overlap downstream of the turbine T2 and onwards, a method was implemented to track the 'center' of the last emitted wake only. Specifically, the wake center was defined as the barycenter of the temporally and spatially filtered streamwise power deficit on the probed surface. This approach, presented in details in Appendix A, proved suitable for both curled and non-curled wakes, and thus relevant for all the configurations studied in this work. Our approach is similar to the 'weighted geometric-center' approach available in the SAMWICH (Simulated And Measured Wake Identification

https://doi.org/10.5194/wes-2026-37
Preprint. Discussion started: 17 February 2026
© Author(s) 2026. CC BY 4.0 License.

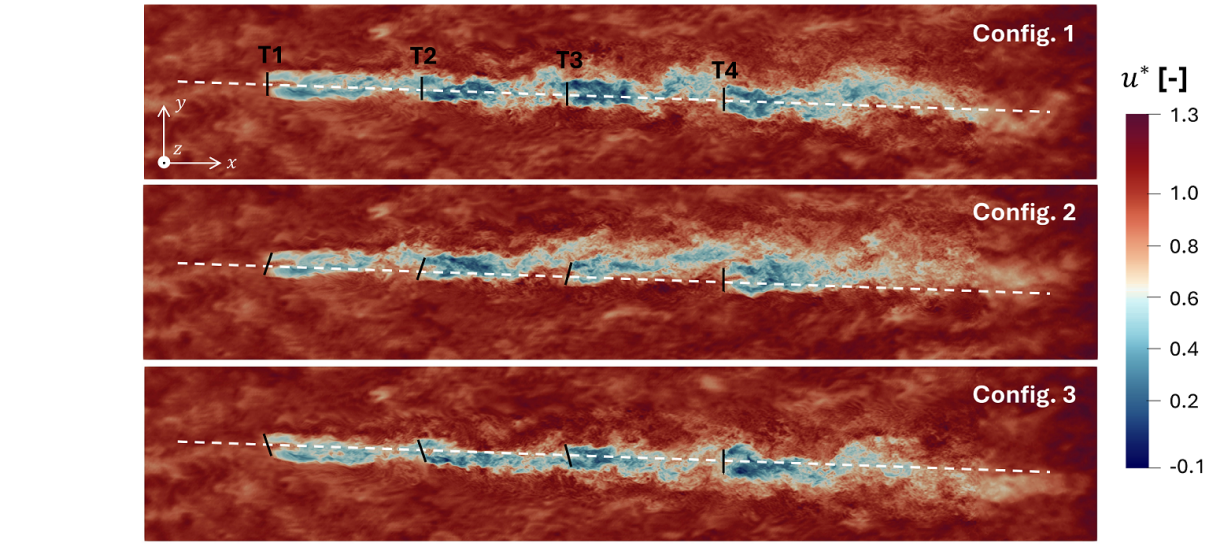

Figure 16. Streamwise velocity $u^* = u/U_\infty$, obtained with YALES2-BHawC at hub height for the configurations 1 to 3 (top to bottom).

and CHaracterization ToolBox) library (Quon et al., 2020), although the implementation details differ. In the following, the instantaneous center $(y_{w,i}, z_{w,i})(t)$ of the wake emitted by the closest upstream turbine i is defined as follows:

$$y_{w,i}(t) = y_i + \langle y_d \rangle_T + y_m(t), \tag{13}$$

$$z_{w,i}(t) = z_i + \langle z_d \rangle_T + z_m(t), \tag{14}$$

where y_i and z_i defines respectively the lateral and vertical coordinate of the upstream rotor center, while y_m and $z_m(t)$ refers to the lateral and vertical instantaneous meandering of the wake, with respect to its lateral $\langle y_d \rangle_T$ and vertical $\langle z_d \rangle_T$ time-averaged deflection.

The mean deflections are first depicted in Fig. 17 for all configurations. Interestingly, a slight crosswise negative deflection is achieved downstream the first turbine in the baseline configuration, even though no yaw command is applied on this turbine. Such deflection was also observed when considering the time-averaged streamwise power deficit in the vertical sampling plane. This result echoes the 'natural deflection' mechanism mentioned in (Fleming et al., 2014), reported to be caused by an interaction of the rotating wake with the ground. Yet, this past observation was made for a veered inflow, thus suggesting a possible statistical artifact (Fleming et al., 2018) in this case. More generally, the results show that the mean achieved deflections are not symmetric with respect to the sign of the yaw commands. Indeed, and despite the deflection being higher in amplitude downstream the first turbine for the configurations 3 and 5, the lateral deflections are higher in the configurations 2 and 4 for the three other turbines. This global behavior of the flow, which contradicts with the behavior of the first wake, is likely to result from the layout orientation. The yaw commands applied in configurations 2 and 4 truly steer the wakes away from the downstream turbines, leading those to operate with a higher wind speed. Consequently, a higher lateral thrust is generated which contributes to deflect the new emitted wake more effectively. While difficult to properly highlight, blockage effects are

https://doi.org/10.5194/wes-2026-37
Preprint. Discussion started: 17 February 2026
© Author(s) 2026. CC BY 4.0 License.

eawe european academy of wind energy
Open Access WIND ENERGY SCIENCE DISCUSSIONS

also likely to be more impacting in configurations 3 and 5. As a result, the secondary wake steering effect on the last turbine T4 shows to be significantly stronger in the configurations 2 and 4.

Consistently with Fig. 12, an upward deflection of the wakes is also present, which shows to be significantly more pronounced in configurations 1, 3, and 5. This can be primarily explained by stronger rotor-wake interactions. Indeed, wake combinations should favor the accumulation of vertical momentum. This is even more plausible as higher thrust forces are applied by each turbine on the flow in configurations 2 and 4, which may have resulted in a higher vertical deflection of the wakes at a given downstream position. Yet, for these two configurations, one can notice in Fig. 12 that the upward vertical movement of each wake results in a downward vertical movement on the sides of the wake. Such region partially impacts each downstream turbine and could limit the upward movement of the next emitted wake.

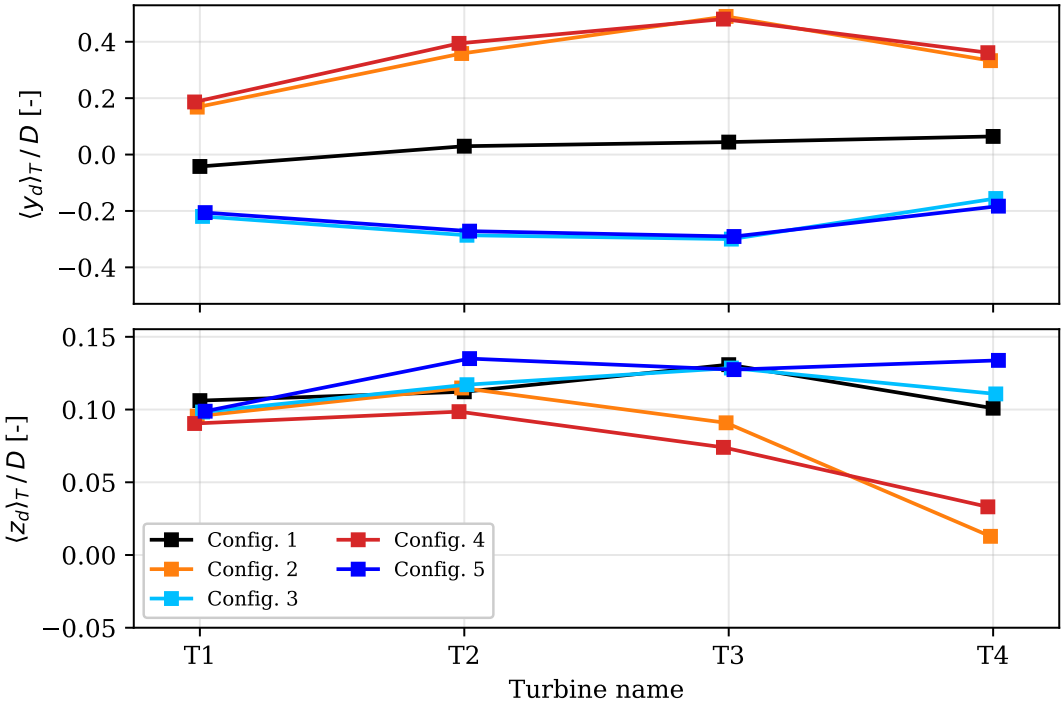

Figure 17. Time-averaged wake deflections $\langle y_d \rangle_T / D$ (top) and $\langle z_d \rangle_T / D$ (bottom) obtained 4 diameters downstream each turbine, for all investigated configurations. The time averaging was performed over the second half of the time period T_s.

The instantaneous meandering amplitudes $y_m(t)$ and $z_m(t)$ obtained for each turbine in configurations 1 to 3 are finally given in Fig. 18. The amplitude of the vertical meandering appears to be half that of the lateral counterpart in configurations 1 and 3. This is caused in part by the bottom boundary of the domain, which constrains the flow movement in the vertical direction. However, this vertical movement shows to amplify after the second turbine. As for the lateral meandering, it is less prominent in configuration 2, as the wakes are already significantly steered towards the ambient background flow. This stands as a clear

https://doi.org/10.5194/wes-2026-37
Preprint. Discussion started: 17 February 2026
© Author(s) 2026. CC BY 4.0 License.

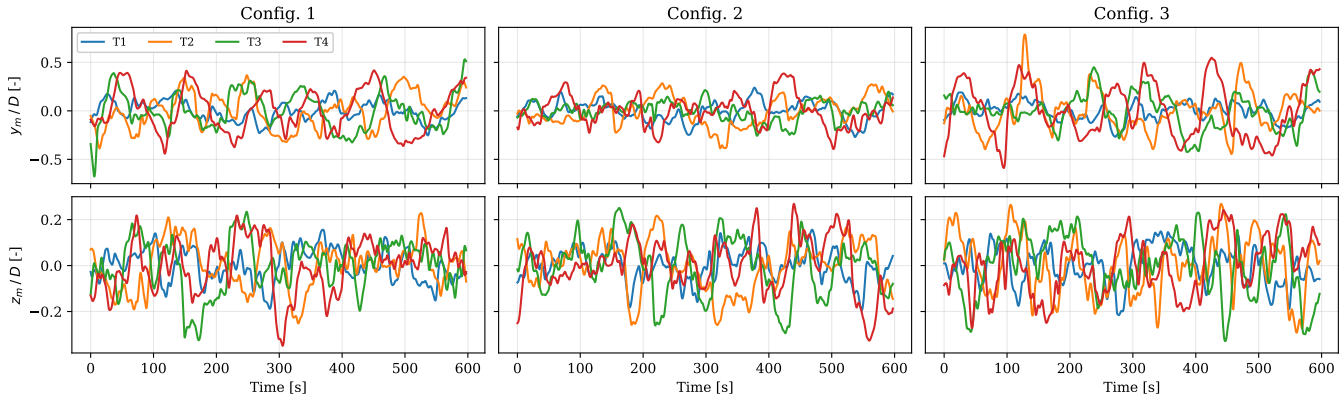

Figure 18. Comparison of the instantaneous meandering amplitudes $y_m(t)$ (top) and $z_m(t)$ (bottom) 4 diameters downstream each turbine, for configurations 1 to 3 (left to right).

difference with respect to configurations 1 and 3, where the lateral meandering amplitude both increases monotonically after each turbine and shows to progressively lock on a preferred natural frequency.

This phenomenon is further emphasized in Fig. 19, where the spectra of $y_m(t)$ and $z_m(t)$ obtained with an FFT are given as a function of the Strouhal number St, here defined as:

$$St = \frac{fD}{U_{\infty,i}}, \tag{15}$$

where $U_{\infty,i}$ is the REWS wind speed obtained $2.5D$ upstream of each turbine i. As mentioned in (Dong et al., 2023), one can identify two main regions in the resulting spectra, approximately delimited by $St = 0.1$. Each region is representative of one of the two main driving mechanisms of the meandering. The spectra part below this threshold is usually driven by the 'inflow large-eddy' mechanism, which is a passive transport of the wake by the largest eddies present in the background flow. In contrast, the remaining part of the spectra, and especially the one attached to the Strouhal number range $[0.1, 0.4]$, is usually representative of the rotor's annular shear layer instability mechanism, governed by scales closer to the rotor diameter. Nonetheless, considering the domain size and the wind speed U_∞ used in this work, those two regions may not be that strictly delimited here. Consistent with Fig. 11, the amplitude of the spectra obtained for $y_m(t)$ shows to increase gradually in the Strouhal number range $[0.1, 0.4]$, specifically in configurations 1 and 3. Interestingly, the contribution attached to lower Strouhal numbers also shows to increase up to the turbine T3, but seems to progressively shift toward the above Strouhal number range, suggesting again a lock-in phenomenon. This is consistent with the idea that the largest incoming eddies may be broken in smaller ones when flowing through a rotor-swept area, leading to a deficit in the large-scale turbulent energy in the wake (Heisel et al., 2018). Indeed, one can expect this effect to be intensified with multiple wind turbines in line. Consequently, the two main mechanisms driving the meandering tends to originate from comparable eddy scales. A similar evolution can be seen in configuration 2, yet to a lesser extent. The results obtained for the last emitted wake still shows an amplification of

https://doi.org/10.5194/wes-2026-37
Preprint. Discussion started: 17 February 2026
© Author(s) 2026. CC BY 4.0 License.

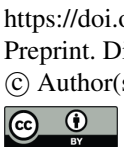

eawe european academy of wind energy
Open Access WIND ENERGY SCIENCE DISCUSSIONS

the meandering, but may be explained by a relaxation of the mean deflection constraint, as no yaw command is applied on the turbine T4.

Considering the spectra obtained from the $z_m(t)$ time series, similar observations and comments can be made for configurations 1 and 3. The results in configuration 2 do not show the same trend, with the wakes respectively emitted by the turbines T1 and T4 showing a similar spectrum amplitude in the meandering Strouhal range. This last observation can be seen as consistent with the time-averaged vertical deflection $\langle z_d \rangle_T$ obtained for the turbine T4 in configuration 2. Indeed, the last wake was shown to move closer to the bottom boundary, which may have constrained the vertical meandering.

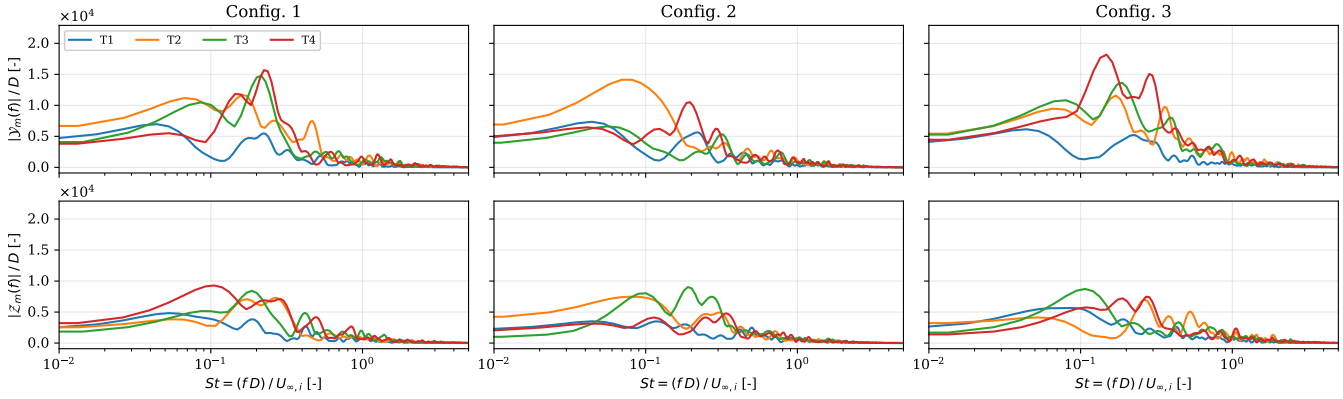

Figure 19. Comparison of the spectra obtained from the instantaneous meandering amplitudes $y_m(t)$ (top) and $z_m(t)$ (bottom) 4 diameters each turbine, for configurations 1 to 3 (left to right).

It is to be emphasized that the previously illustrated ramp-up of the meandering amplitude along the turbine row is not factored in as such in the common engineering models. Especially, the widely used wake-added turbulence model (Crespo and Hernandez, 1996) considers only a decay of the wake added turbulence as a function of the downstream distance. Although it is commonly admitted that the added-turbulence generated in the near wake, from the pairing and breakdown of the tip vortices, will decay in the far wake, the added turbulence resulting from the increasing meandering motion in the far wake partially compensates. In the scenario investigated in this work, this compensation grows even stronger, which questions the model formulation.

5 Conclusions

This work focused on the open-loop implementation of wake steering control. A 4-turbine row layout was examined, corresponding to a part of an existing offshore wind farm. Several configurations relevant for the design of wake steering strategies were looked at, by running both LES simulations and simulations with engineering wake models. We stress that the latter wake models were used with their default parameter sets, which are coming from the original literature. All yaw commands applied in the simulations were derived using the optimization framework proposed in (Rott et al., 2018), which relies on engineering

https://doi.org/10.5194/wes-2026-37
Preprint. Discussion started: 17 February 2026
© Author(s) 2026. CC BY 4.0 License.

eawe european academy of wind energy
Open Access WIND ENERGY SCIENCE DISCUSSIONS

wake models for affordability and aims to increase the optimization robustness with respect to the turbulence-induced wind direction variability. The free-stream wind speed at hub height U_∞ and the layout orientation α_0 were specifically chosen to focus on the operating conditions where the highest absolute power benefit is achieved, according to the engineering wake models. Furthermore, a 6.5% turbulence intensity at hub height was used, as often met in the offshore domain. Nonetheless, the main limitation of the study definitely lies in the inflow considered for all the LES configurations. Only a truly neutral atmospheric boundary layer was simulated to reduce the requirements in computational resources. Consequently, although partly supported by previous findings from the literature, the observations presented in this work would require further consolidation. Supplementary studies, aiming to explore different atmospheric conditions but also different layout, are already planned to this end and should occur in the near future.

To build upon prior studies from the literature, the specific case of a $+4°$ static error on the absolute wind direction was investigated in this work. For the considered layout and its orientation, this bias led to select yaw commands similar to the optimal ones in magnitude, but of opposite sign. For this very unfavorable case, both the wake model and the LES predicted a slight power loss relative to the baseline case, instead of the $\sim 20\%$ gain obtained with the optimal commands, highlighting once more the high sensitivity of wake steering control to the absolute wind direction. Notably, a $-4°$ static error would have produced yaw settings nearly identical to the optimal case and therefore no significant reduction of the power benefit.

The present study also considered yaw application errors on all the turbines, representing a typical nacelle positioning uncertainty, likely to happen in the field in case of time-varying wind conditions. An error of -2° was considered on all the turbines for simplicity. This scenario showed the total power production to be only marginally altered when yaw commands were applied, outcome somewhat expected as this error was 7 to 10 times smaller than all non-zero yaw commands.

The wake models and LES produced similar predictions of power gains and losses, both at the turbine and farm level. Especially, and when truly applying the optimum yaw commands, the simulations all emphasized that the largest part of the power benefit was obtained on the most downstream turbines and thus more challenging to achieve in the field where the wind conditions may deviate from the idealized ones. Nonetheless, per-turbine power differences were observed, particularly noticeable for the most downstream turbine. The LES results also revealed context-dependent modeling biases, mainly related to the degree of wake overlap. In case of strong wake combinations, the wake meandering in the LES simulations was observed to ramp up in magnitude along the turbine row, while also progressively locking on the Strouhal number range $[0.1, 0.4]$. This effect is typically not addressed in the wake models. Furthermore, this behavior also makes the practical quantification of the power benefit challenging in the field. Indeed, considering again that the benefit is mostly achieved on the most downstream turbines, this means that the gain assessment reference period should ideally encompass several cycles of the meandering in this area of the farm for the baseline case. Depending on the local wind speed in this area, this reference period may be to long to verify statistically steady wind conditions. As an alternative, collecting 1-minute samples for both the baseline and optimized operation modes was shown, according to a bootstrap procedure made with the LES results, to lead to a reasonably small variability of the estimated power gain, even with only 5 samples available from each operation mode. Yet it is stressed that this procedure was performed in idealized conditions for the optimized mode, as all samples were obtained while the wake deflections were fully active. Considering the time required to converge the flow in the field after implementing yaw

https://doi.org/10.5194/wes-2026-37
Preprint. Discussion started: 17 February 2026
© Author(s) 2026. CC BY 4.0 License.

commands, such ideal 1-minute samples may still be difficult to collect. In partial wake overlap cases, LES also indicated a faster decay of the wake added turbulence and a persisting velocity deficit, which were again poorly represented by the wake models. Such shortcomings of the wake models therefore add a modeling-based uncertainty in the yaw optimization tool chain.

Overall, these findings further stress the intrinsic challenges of open-loop wake steering control, especially when relying on simplified wake models and idealized wind conditions. Yet, considering how easier the open-loop approaches are to implement, compared to the closed-loop counterparts (Meyers et al., 2022), seeking to improve and develop open-loop solutions remains legitimate. In light of the obtained results, several improvement pathways would deserve additional exploration:

- Wake modeling: developing wake models that incorporate more physics (Martínez-Tossas et al., 2019, 2021; Bay et al., 2023) remains essential. As proposed here and in previous works, comparisons with LES for configurations representative of farm control scenarios can guide and validate such developments.

- Calibration of absolute wind direction: improving calibration accuracy and minimizing the residual static bias should be a priority. In place of the SCADA-based calibration procedures, yet convenient, GPS instruments or even satellite images could be used to sharpen the initial calibration (Bromm et al., 2018), albeit with a higher cost and operational complexity. Still, this first calibration should remained followed by a continuous monitoring to detect and correct a progressive or sudden drift, or to compensate for unavailable measurements. Consensus-based strategies can address these issues (Annoni et al., 2019). A full-farm update of the calibration should also be performed periodically and after major maintenance operations.

- Robustness of optimal yaw commands: the robustness of optimal yaw settings to static wind direction errors should be explicitly considered. The approach from (Rott et al., 2018) could be extended by convolving the Gaussian distribution representing dynamic errors with an additional distribution for static biases, such asPowe for instance a rectangular distribution over $[-2W_{d,tol}, 2W_{d,tol}]$, where $W_{d,tol}$ would be a tolerance defined in the monitoring design to detect a drifting calibration. This additional distribution could also be turbine-specific to account for local effects such as increased turbulence or greater calibration uncertainty. It is noteworthy that this approach could also be applied to tackle the wind speed uncertainty. However, all these enhancements, while helping to secure a positive power benefit, may also considerably reduce the reachable value of this benefit.

- Field application criteria: operational criteria are usually defined to prevent control activation under conditions inconsistent with model assumptions (e.g., turbines offline). Additionally, wake detection techniques, based on turbine SCADA data (Bottasso et al., 2018; Fojcik et al., 2025), or LiDAR measurements (Aitken et al., 2014; Raach et al., 2017; Lio et al., 2021), could serve both as safeguards and as means to refine yaw settings according to local conditions. Although approaching closed-loop concepts, such methods could still be integrated within an open-loop framework.

https://doi.org/10.5194/wes-2026-37
Preprint. Discussion started: 17 February 2026
© Author(s) 2026. CC BY 4.0 License.

eawe european academy of wind energy
Open Access WIND ENERGY SCIENCE DISCUSSIONS

Appendix A: Wake tracking

For the purpose of quantifying the meandering of the wake emitted by the closest upstream wind turbine, a wake tracking approach was implemented. In this approach, the wake center was defined as the barycenter of the 'power deficit'. All steps followed to derive it are illustrated in Fig. A1, considering the wake emitted by the leading turbine in configuration 2 from Table 1. Starting from an initial velocity field $u^* = u/U_\infty$, as sampled at time t in a finite cross-flow plane, a time averaging is first applied to get the field $\langle u^* \rangle_{T=\Delta t}$ on the sampling grid. This is achieved by considering all flow snapshots sampled in the time window $[t - \Delta t/2, t + \Delta t/2]$. In this work, the width of the time window was set $\Delta t = 4.0$ s, for a sampling period of 0.4 s. The normalized power deficit ΔP_0^* is then defined as follows:

$$\Delta P_0^* = 100 \max\left(0, \left(\frac{\langle u^* \rangle_{T,0} - \langle u^* \rangle_{T=\Delta t}}{\langle u^* \rangle_{T,0}}\right)^3\right), \tag{A1}$$

where $\langle u^* \rangle_{T,0}$ is the free-stream velocity, averaged in time over a period T, set in this work to 600 s. The power deficit field is subsequently truncated by resetting to 0 all values that are below the 90% percentile q_{90}. This operation acts as a simple way to reject local non-relevant power deficits, which may typically emerge close to the ground or in a region waked by another upstream turbine. Other truncation operations can optionally be applied, either for the full tracking or locally in time, to further prevent the wake center from suddenly jumping to a spurious location. As a last preparation step, the resulting power deficit field ΔP_1^* is spatially filtered using a Gaussian kernel G of standard deviation $\sigma_G = 0.1D$, yielding the final deficit field ΔP_2^*. The wake center coordinates $(y_w, z_w)(t)$ at time t are finally calculated as:

$$(y_w, z_w)(t) = \left(\frac{\sum_k y_k \, \Delta P_{2,k}^*(t)}{\sum_k \Delta P_{2,k}^*(t)}, \frac{\sum_k z_k \, \Delta P_{2,k}^*(t)}{\sum_k \Delta P_{2,k}^*(t)}\right), \tag{A2}$$

where the index k refers to a point of the sampling grid.

Code availability. BHawC code (Rubak and Petersen, 2005) is proprietary software of the Siemens Gamesa Renewable Energy company, and its source code is strictly confidential. The YALES2 code (Moureau et al., 2011) is the property of CNRS (Centre National de la Recherche Scientifique); it is freely shared for academic studies and has a public website (Moureau et al., 2025).

Data availability. The raw field data used in this work have been generously provided to the authors by the wind farm owner (which shall remain anonymous), and remain its private property. It is therefore not possible for the authors to disclose it. Similarly, all numerical results provided by YALES2 and BHawC cannot be shared for confidentiality reasons related to the simulated turbine design and wind farm.

.

https://doi.org/10.5194/wes-2026-37
Preprint. Discussion started: 17 February 2026
© Author(s) 2026. CC BY 4.0 License.

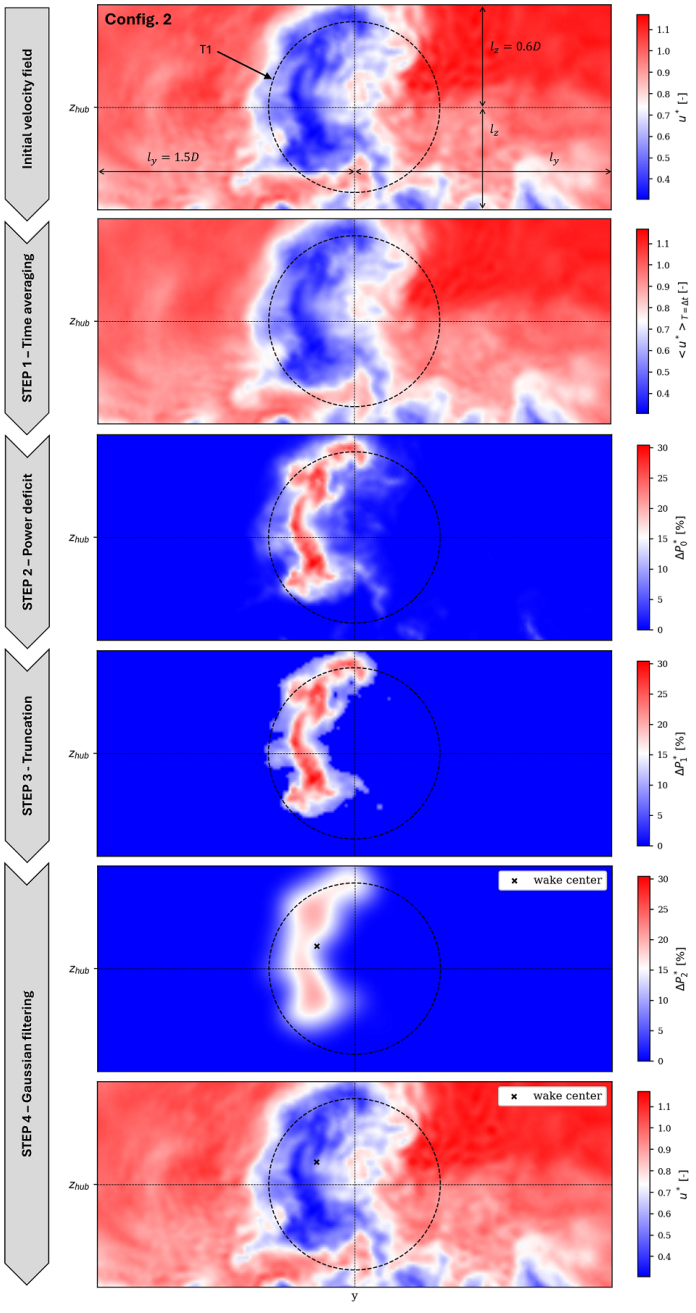

Figure A1. Overview of the successive steps involved in the wake tracking methodology considered in this work. In this example, the initial flow field was sampled 4 diameters downstream the turbine T1, in the studied configuration 2 from Table 1.

https://doi.org/10.5194/wes-2026-37
Preprint. Discussion started: 17 February 2026
© Author(s) 2026. CC BY 4.0 License.

eawe european academy of wind energy
Open Access WIND ENERGY SCIENCE DISCUSSIONS

Author contributions. All authors were involved in the conceptualization of the study. EM and JC selected the wind direction and nacelle positioning errors used in this work, and proposed the improvements pathways for open-loop wake steering control. EM and SG reviewed the existing literature. The overall LES simulation methodology was designed and developed by EM, SG and FHM. LAMT provided valuable advice on how to prepare and run the precursor simulation in particular. EM, SG and FHM implemented and verified the required software developments for the YALES2-BHawC coupling. LB implemented the pre-processing framework for the SCADA data, which was then used by EM to validate the no-control case with filtered SCADA data. EM set up and run all simulations, performed the post-processing actions, generated all plots and visuals and conducted the subsequent analysis. EM and SG wrote and edited the manuscript. All co-authors reviewed the original draft. LB, LAMT and PB supervised this work.

Competing interests. Laurent Beaudet, Juliette Coussy declare that they were fulltime employees of Siemens Gamesa Renewable Energy at the time this work was carried out. As part of a sabbatical, Louis A. Martinez-Tossas also declares that he was working four days a week for Siemens Gamesa Renewable Energy during this period.

Acknowledgements. This project was provided with computer and storage resources by GENCI at TGCC thanks to the grants 2024-A0162A11335 and 2025-A0182A11335 on the supercomputer Joliot Curie's ROME partition, and to CRIANN resources under the allocation 2012006.

Financial support. This work is funded, in part, by Région Normandie and the ERDF fund via the "I-Démo" SCALE OP project under convention 00152289 ("I-Démo", France, BPI France and France 2030 AAP).

https://doi.org/10.5194/wes-2026-37
Preprint. Discussion started: 17 February 2026
© Author(s) 2026. CC BY 4.0 License.

eawe european academy of wind energy
Open Access WIND ENERGY SCIENCE DISCUSSIONS

References

Aitken, M. L., Banta, R. M., Pichugina, Y. L., and Lundquist, J. K.: Quantifying wind turbine wake characteristics from scanning remote sensor data, Journal of Atmospheric and Oceanic Technology, 31, 765–787, https://doi.org/10.1175/JTECH-D-13-00104.1, 2014.

Annoni, J., Bay, C., Johnson, K., Dall'Anese, E., Quon, E., Kemper, T., and Fleming, P.: Wind direction estimation using SCADA data with consensus-based optimization, Wind Energy Science, 4, 355–368, https://doi.org/10.5194/wes-4-355-2019, 2019.

Bastankhah, M. and Porté-Agel, F.: Experimental and theoretical study of wind turbine wakes in yawed conditions, Journal of Fluid Mechanics, 806, 506–541, https://doi.org/10.1017/jfm.2016.595, 2016.

Bay, C. J., Fleming, P., Doekemeijer, B., King, J., Churchfield, M., and Mudafort, R.: Addressing deep array effects and impacts to wake steering with the cumulative-curl wake model, Wind Energy Science Discussions, 8, 401–419, https://doi.org/10.5194/wes-8-401-2023, 2023.

Bénard, P., Viré, A., Moureau, V., Lartigue, G., Beaudet, L., Deglaire, P., and Bricteux, L.: Large-eddy simulation of wind turbines wakes including geometrical effects, Computers & Fluids, 173, 133–139, https://doi.org/10.1016/j.compfluid.2018.03.015, 2018.

Bossanyi, E.: Combining induction control and wake steering for wind farm energy and fatigue loads optimisation, Journal of Physics: Conference Series, 1037, 032 011, https://doi.org/10.1088/1742-6596/1037/3/032011, 2018.

Bottasso, C., Cacciola, S., and Schreiber, J.: Local wind speed estimation, with application to wake impingement detection, Renewable Energy, 116, 155–168, https://doi.org/10.1016/j.renene.2017.09.044, 2018.

Bromm, M., Rott, A., Beck, H., Vollmer, L., Steinfeld, G., and Kühn, M.: Field investigation on the influence of yaw misalignment on the propagation of wind turbine wakes, Wind Energy, 21, 1011–1028, https://onlinelibrary.wiley.com/doi/abs/10.1002/we.2210, 2018.

Campagnolo, F., Petrović, V., Bottasso, C. L., and Croce, A.: Wind tunnel testing of wake control strategies, in: 2016 American Control Conference (ACC), pp. 513–518, https://doi.org/10.1109/ACC.2016.7524965, 2016.

Campagnolo, F., Weber, R., Schreiber, J., and Bottasso, C. L.: Wind tunnel testing of wake steering with dynamic wind direction changes, Wind Energy Science Discussions, 2020, 1–33, https://doi.org/10.5194/wes-5-1273-2020, 2020.

Cao, L., Ge, M., Gao, X., Du, B., Li, B., Huang, Z., and Liu, Y.: Wind farm layout optimization to minimize the wake induced turbulence effect on wind turbines, Applied Energy, 323, 119 599, https://doi.org/10.1016/j.apenergy.2022.119599, 2022.

Chorin, A. J.: Numerical solution of the Navier-Stokes equations, Mathematics of computation, 22, 745–762, 1968.

Crespo, A. and Hernandez, J.: Turbulence characteristics in wind-turbine wakes, Journal of wind engineering and industrial aerodynamics, 61, 71–85, https://doi.org/10.1016/0167-6105(95)00033-X, 1996.

Dapogny, C., Dobrzynski, C., and Frey, P.: Three-dimensional adaptive domain remeshing, implicit domain meshing, and applications to free and moving boundary problems, Journal of computational physics, 262, 358–378, https://doi.org/10.1016/j.jcp.2014.01.005, 2014.

Doekemeijer, B. M., van der Hoek, D., and van Wingerden, J.-W.: Closed-loop model-based wind farm control using FLORIS under time-varying inflow conditions, Renewable Energy, 156, 719–730, https://doi.org/10.1016/j.renene.2020.04.007, 2020.

Doekemeijer, B. M., Kern, S., Maturu, S., Kanev, S., Salbert, B., Schreiber, J., Campagnolo, F., Bottasso, C. L., Schuler, S., Wilts, F., et al.: Field experiment for open-loop yaw-based wake steering at a commercial onshore wind farm in Italy, Wind Energy Science, 6, 159–176, https://doi.org/10.5194/wes-6-159-2021, 2021.

Doekemeijer, B. M., Simley, E., and Fleming, P.: Comparison of the Gaussian wind farm model with historical data of three offshore wind farms, Energies, 15, 1964, https://doi.org/10.3390/en15061964, 2022.

https://doi.org/10.5194/wes-2026-37
Preprint. Discussion started: 17 February 2026
© Author(s) 2026. CC BY 4.0 License.

Dong, G., Qin, J., Li, Z., and Yang, X.: Characteristics of wind turbine wakes for different blade designs, Journal of Fluid Mechanics, 965, A15, https://doi.org/10.1017/jfm.2023.385, 2023.

Energy Institute: 2024 Statistical Review of World Energy, https://assets.kpmg.com/content/dam/kpmg/az/pdf/2024/Statistical-Review-of-World-Energy.pdf, (last access: 30 October 2025), 2024.

Fleming, P., Gebraad, P. M., Lee, S., van Wingerden, J.-W., Johnson, K., Churchfield, M., Michalakes, J., Spalart, P., and Moriarty, P.: Simulation comparison of wake mitigation control strategies for a two-turbine case, Wind Energy, 18, 2135–2143, https://doi.org/10.1002/we.1810, 2015.

Fleming, P., Annoni, J., Shah, J. J., Wang, L., Ananthan, S., Zhang, Z., Hutchings, K., Wang, P., Chen, W., and Chen, L.: Field test of wake steering at an offshore wind farm, Wind Energy Science, 2, 229–239, https://doi.org/10.5194/wes-2-229-2017, 2017.

Fleming, P., Annoni, J., Churchfield, M., Martinez-Tossas, L. A., Gruchalla, K., Lawson, M., and Moriarty, P.: A simulation study demonstrating the importance of large-scale trailing vortices in wake steering, Wind Energy Science, 3, 243–255, https://doi.org/10.5194/wes-3-243-2018, 2018.

Fleming, P., King, J., Dykes, K., Simley, E., Roadman, J., Scholbrock, A., Murphy, P., Lundquist, J. K., Moriarty, P., Fleming, K., et al.: Initial results from a field campaign of wake steering applied at a commercial wind farm–Part 1, Wind Energy Science, 4, 273–285, https://doi.org/10.5194/wes-4-273-2019, 2019.

Fleming, P. A., Gebraad, P. M., Lee, S., van Wingerden, J.-W., Johnson, K., Churchfield, M., Michalakes, J., Spalart, P., and Moriarty, P.: Evaluating techniques for redirecting turbine wakes using SOWFA, Renewable Energy, 70, 211–218, https://doi.org/10.1016/j.renene.2014.02.015, 2014.

Fleming, P. A., Stanley, A. P. J., Bay, C. J., King, J., Simley, E., Doekemeijer, B. M., and Mudafort, R.: Serial-Refine Method for Fast Wake-Steering Yaw Optimization, Journal of Physics: Conference Series, 2265, 032 109, https://doi.org/10.1088/1742-6596/2265/3/032109, 2022.

Fojcik, P., Hart, E., and Hedevang, E.: Wind turbine wake detection and characterisation utilising blade loads and SCADA data: a generalised approach, Wind Energy Science Discussions, 2025, 1–37, https://doi.org/10.5194/wes-10-1943-2025, 2025.

Gebraad, P. M., Teeuwisse, F. W., Van Wingerden, J., Fleming, P. A., Ruben, S. D., Marden, J. R., and Pao, L. Y.: Wind plant power optimization through yaw control using a parametric model for wake effects—a CFD simulation study, Wind Energy, 19, 95–114, https://doi.org/10.1002/we.1822, 2016.

Göçmen, T., Campagnolo, F., Duc, T., Eguinoa, I., Andersen, S. J., Petrović, V., Imširović, L., Braunbehrens, R., Liew, J., Baungaard, M., et al.: FarmConners wind farm flow control benchmark–Part 1: Blind test results, Wind Energy Science, 7, 1791–1825, https://doi.org/10.5194/wes-7-1791-2022, 2022.

Heisel, M., Hong, J., and Guala, M.: The spectral signature of wind turbine wake meandering: A wind tunnel and field-scale study, Wind Energy, 21, 715–731, https://doi.org/10.1002/we.2189, 2018.

Hodgson, E. L. and Andersen, S. J.: Wake steering under inflow wind direction uncertainty: an LES study, Wind Energy Science Discussions, 2025, 1–26, https://doi.org/10.5194/wes-2025-243, 2025.

Houtin-Mongrolle, F.: Investigations of yawed offshore wind turbine interactions through aero-servo-elastic Large Eddy Simulations, Ph.D. thesis, Normandie Université, https://theses.hal.science/tel-03987411, (last access: 30 October 2025), 2022.

International Energy Agency: World Energy Outlook 2024, https://www.iea.org/reports/world-energy-outlook-2024, (last access: 30 October 2025), 2024.

https://doi.org/10.5194/wes-2026-37
Preprint. Discussion started: 17 February 2026
© Author(s) 2026. CC BY 4.0 License.

Jensen, N.: A note on wind generator interaction, no. 2411 in Risø-M, Risø National Laboratory, ISBN 87-550-0971-9, https://backend.orbit.dtu.dk/ws/portalfiles/portal/55857682/ris_m_2411.pdf, 1983.

Jiménez, Á., Crespo, A., and Migoya, E.: Application of a LES technique to characterize the wake deflection of a wind turbine in yaw, Wind energy, 13, 559–572, https://doi.org/10.1002/we.380, 2010.

King, J., Fleming, P., King, R., Martínez-Tossas, L. A., Bay, C. J., Mudafort, R., and Simley, E.: Control-oriented model for secondary effects of wake steering, Wind Energy Science, 6, 701–714, https://wes.copernicus.org/articles/6/701/2021/, 2021.

Kraushaar, M.: Application of the compressible and low-Mach number approaches to Large-Eddy Simulation of turbulent flows in aero-engines, Ph.D. thesis, Institut National Polytechnique de Toulouse-INPT, https://theses.hal.science/tel-00711480, (last access: 30 October 2025), 2011.

Lilly, D. K.: A proposed modification of the Germano subgrid-scale closure method, Physics of Fluids A: Fluid Dynamics, 4, 633–635, https://doi.org/10.1063/1.858280, 1992.

Lio, W. H., Larsen, G. C., and Thorsen, G. R.: Dynamic wake tracking using a cost-effective LiDAR and Kalman filtering: Design, simulation and full-scale validation, Renewable Energy, 172, 1073–1086, https://doi.org/10.1016/j.renene.2021.03.081, 2021.

Liu, Y., Ding, L., Yu, Z., Xiao, T., Lu, Q., Chen, Y., and Wang, W.: Maximizing Wind Farm Power Output through Site-Specific Wake Model Calibration and Yaw Optimization, Energy Engineering, 122, 4365–4384, https://doi.org/10.32604/ee.2025.068712, 2025.

Malandain, M., Maheu, N., and Moureau, V.: Optimization of the deflated conjugate gradient algorithm for the solving of elliptic equations on massively parallel machines, Journal of Computational Physics, 238, 32–47, https://doi.org/10.1016/j.jcp.2012.11.046, 2013.

Martínez-Tossas, L. A., Annoni, J., Fleming, P. A., and Churchfield, M. J.: The aerodynamics of the curled wake: a simplified model in view of flow control, Wind Energy Science, 4, 127–138, https://doi.org/10.5194/wes-4-127-2019H, 2019.

Martínez-Tossas, L. A., King, J., Quon, E., Bay, C. J., Mudafort, R., Hamilton, N., Howland, M. F., and Fleming, P. A.: The curled wake model: a three-dimensional and extremely fast steady-state wake solver for wind plant flows, Wind Energy Science, 6, 555–570, https://doi.org/10.5194/wes-6-555-2021, 2021.

Meyers, J., Bottasso, C., Dykes, K., Fleming, P., Gebraad, P., Giebel, G., Göçmen, T., and Van Wingerden, J.-W.: Wind farm flow control: prospects and challenges, Wind Energy Science Discussions, 2022, 1–56, https://doi.org/10.5194/wes-7-2271-2022, 2022.

Mittelmeier, N. and Kühn, M.: Determination of optimal wind turbine alignment into the wind and detection of alignment changes with SCADA data, Wind Energy Science, 3, 395–408, https://doi.org/10.5194/wes-3-395-2018, 2018.

Moureau, V., Domingo, P., and Vervisch, L.: Design of a massively parallel CFD code for complex geometries, Comptes rendus. Mécanique, 339, 141–148, 2011.

Moureau, V., Lartigue, G., Bénard, P., and Bioche, K.: YALES2 public page, https://www.coria-cfd.fr/index.php/YALES2, (last access: 30 October 2025), 2025.

Muller, E., Gremmo, S., Houtin-Mongrolle, F., Duboc, B., and Bénard, P.: Field-data-based validation of an aero-servo-elastic solver for high-fidelity large-eddy simulations of industrial wind turbines, Wind Energy Science, 9, 25–48, https://doi.org/10.5194/wes-9-25-2024, 2024.

Munters, W. and Meyers, J.: Dynamic strategies for yaw and induction control of wind farms based on large-eddy simulation and optimization, Energies, 11, 177, https://doi.org/10.3390/en11010177, 2018.

Murcia, J. P., Réthoré, P.-E., Hansen, K. S., Natarajan, A., and Sørensen, J. D.: A new method to estimate the uncertainty of AEP of offshore wind power plants applied to Horns Rev 1, in: EWEA Annual Conference and Exhibition 2015, pp. 161–165, ISBN 9782930670003, https://backend.orbit.dtu.dk/ws/portalfiles/portal/123965472/EWEA_paper_jumu.pdf, 2015.

https://doi.org/10.5194/wes-2026-37
Preprint. Discussion started: 17 February 2026
© Author(s) 2026. CC BY 4.0 License.

National Laboratory of the Rockies (NLR): FLORIS (version 4.2.2), https://github.com/NREL/floris/tree/v4.2.2, (last access: 12 December 2025), 2024.

National Laboratory of the Rockies (NLR): FLORIS documentation (Wake Combination Models), https://nrel.github.io/floris/wake_models.html#wake-combination-models, (last access: 12 December 2025), 2025.

Niayifar, A. and Porté-Agel, F.: Analytical modeling of wind farms: A new approach for power prediction, Energies, 9, 741, https://doi.org/10.3390/en9090741, 2016.

Patel, A., Muller, E., and Houtin-Mongrolle, F.: Towards an automated framework for Aero-Servo-Elastic Large Eddy Simulation of wind turbine wakes, Journal of Physics: Conference Series, 2767, 052 059, https://doi.org/10.1088/1742-6596/2767/5/052059, 2024.

Pena Martinez, J. J. and Coussy, J.: Wake steering experiments in onshore and offshore wind farms, Journal of Physics: Conference Series, 2767, 092 090, https://doi.org/10.1088/1742-6596/2767/9/092090, 2024.

Quick, J., Annoni, J., King, R., Dykes, K., Fleming, P., and Ning, A.: Optimization Under Uncertainty for Wake Steering Strategies, Journal of Physics: Conference Series, 854, 012 036, https://doi.org/10.1088/1742-6596/854/1/012036, 2017.

Quick, J., Mouradi, R.-S., Devesse, K., Mathieu, A., Paul Van Der Laan, M., Murcia Leon, J. P., and Schulte, J.: Verification and Validation of Wind Farm Flow Models, Journal of Physics: Conference Series, 2767, 092 074, https://doi.org/10.1088/1742-6596/2767/9/092074, 2024.

Quon, E. W., Doubrawa, P., and Debnath, M.: Comparison of Rotor Wake Identification and Characterization Methods for the Analysis of Wake Dynamics and Evolution, Journal of Physics: Conference Series, 1452, 012 070, https://doi.org/10.1088/1742-6596/1452/1/012070, 2020.

Raach, S., Schlipf, D., and Cheng, P. W.: Lidar-based wake tracking for closed-loop wind farm control, Wind Energy Science, 2, 257–267, https://doi.org/10.5194/wes-2-257-2017, 2017.

Réthoré, P.-E., Johansen, N. A., Frandsen, S. T., Barthelmie, R., Hansen, K., Jensen, L., Bækgaard, M. A., and Kristoffersen, J.: Systematic wind farm measurement data reinforcement tool for wake model calibration, in: European Offshore Wind Conference, pp. 1–10, https://backend.orbit.dtu.dk/ws/portalfiles/portal/6410426/frandsen2_offshore_paper.pdf, 2009.

Rott, A., Doekemeijer, B., Seifert, J. K., van Wingerden, J.-W., and Kühn, M.: Robust active wake control in consideration of wind direction variability and uncertainty, Wind energy science, 3, 869–882, https://doi.org/10.5194/wes-3-869-2018, 2018.

Rubak, R. and Petersen, J. T.: Monopile as part of aeroelastic wind turbine simulation code, in: Copenhagen Offshore Wind Conference, vol. 20, https://www.researchgate.net/publication/242570784_Monopile_as_Part_of_Aeroelastic_Wind_Turbine_Simulation_Code, (last access: 30 October 2025), 2005.

Shakoor, R., Hassan, M. Y., Raheem, A., and Wu, Y.-K.: Wake effect modeling: A review of wind farm layout optimization using Jensen's model, Renewable and Sustainable Energy Reviews, 58, 1048–1059, https://doi.org/10.1016/j.rser.2015.12.229, 2016.

Simley, E., Fleming, P., and King, J.: Design and analysis of a wake steering controller with wind direction variability, Wind Energy Science, 5, 451–468, https://doi.org/10.5194/wes-5-451-2020, 2020.

Simley, E., Fleming, P., Girard, N., Alloin, L., Godefroy, E., and Duc, T.: Results from a wake-steering experiment at a commercial wind plant: investigating the wind speed dependence of wake-steering performance, Wind Energy Science, 6, 1427–1453, https://doi.org/10.5194/wes-6-1427-2021, 2021.

Simley, E., Debnath, M., and Fleming, P.: Investigating the impact of atmospheric conditions on wake-steering performance at a commercial wind plant, Journal of Physics: Conference Series, 2265, 032 097, https://doi.org/10.1088/1742-6596/2265/3/032097, 2022.

https://doi.org/10.5194/wes-2026-37
Preprint. Discussion started: 17 February 2026
© Author(s) 2026. CC BY 4.0 License.

Skjoldan, P. F.: Aeroelastic modal dynamics of wind turbines including anisotropic effects, Ph.D. thesis, Danmarks Tekniske Universitet, ISBN 978-87-550-3848-6, https://backend.orbit.dtu.dk/ws/portalfiles/portal/5509069/ris-phd-66.pdf, (last access: 30 October 2025), 2011.

Sørensen, J. N. and Shen, W. Z.: Numerical Modeling of Wind Turbine Wakes, Journal of Fluids Engineering, 124, 393, https://doi.org/10.1115/1.1471361, 2002.

Steiner, J., Hodgson, E. L., van der Laan, M. P., Alcayaga, L., Pedersen, M., Andersen, S. J., Larsen, G., and Réthoré, P.-E.: A multi-fidelity model benchmark for wake steering of a large turbine in a neutral ABL, Wind Energy Science Discussions, 2025, 1–32, https://doi.org/10.5194/wes-2025-200, 2025.

Stevens, R. J., Martínez-Tossas, L. A., and Meneveau, C.: Comparison of wind farm large eddy simulations using actuator disk and actuator line models with wind tunnel experiments, Renewable energy, 116, 470–478, https://doi.org/10.1016/j.renene.2017.08.072, 2018.

Stipa, S., Ajay, A., Allaerts, D., and Brinkerhoff, J.: TOSCA–an open-source, finite-volume, large-eddy simulation (LES) environment for wind farm flows, Wind Energy Science, 9, 297–320, https://doi.org/10.5194/wes-9-297-2024, 2024.

Van Beek, M. T., Viré, A., and Andersen, S. J.: Sensitivity and uncertainty of the floris model applied on the lillgrund wind farm, Energies, 14, 1293, https://doi.org/10.3390/en14051293, 2021.

van Binsbergen, D., Daems, P.-J., Verstraeten, T., Nejad, A. R., and Helsen, J.: Hyperparameter tuning framework for calibrating analytical wake models using SCADA data of an offshore wind farm, Wind Energy Science, 9, 1507–1526, https://doi.org/10.5194/wes-9-1507-2024, 2024.

Vollmer, L., Steinfeld, G., Heinemann, D., and Kühn, M.: Estimating the wake deflection downstream of a wind turbine in different atmospheric stabilities: an LES study, Wind Energy Science, 1, 129–141, https://doi.org/10.5194/wes-1-129-2016, 2016.

Zhang, J. and Zhao, X.: Quantification of parameter uncertainty in wind farm wake modeling, Energy, 196, 117 065, https://doi.org/10.1016/j.energy.2020.117065, 2020.